ANUL XLVII **2002**

S T U D I A
UNIVERSITATIS BABEŞ-BOLYAI

PHYSICA

2

EDITORIAL OFFICE: Gh. Bilaşcu no. 24, 3400 Cluj-Napoca • Phone 0264-40.53.52

SUMAR - CONTENTS - SOMMAIRE - INHALT

STUDIA UNIVERSITATIS BABEŞ-BOLYAI, PHYSICA, XLVII, 2, 2002

STRUCTURAL AND DIELECTRICAL PROPERTIES OF $Pb_2Mg_{1-x}Co_xWO_6$ SOLID SOLUTIONS

I. ARDELEAN, I. BARBUR, GH. BORODI*, A. VERES, R. VERES and V. TIMAR

Faculty of Physics, "Babes-Bolyai" University, 3400 Cluj-Napoca, Romania
** Institute of Isotopic and Molecular Technologies, 3400 Cluj-Napoca, Romania*

ABSTRACT. X-ray diffraction and dielectric permitivity data performed on $Pb_2Mg_{1-x}Co_xWO_6$ solid solutions with $0 \le x \le 0.3$ are reported. By partial cobalt substitution for magnesium the diffraction patterns are similar to that of Pb_2MgWO_6 compound with a small increase of lattice parameters, which is probable due to the difference in the ionic radii of Mg^{2+} and Co^{2+}. Dielectric anomaly at T_c (38^oC) related to the antiferroelectric transition in Pb_2MgWO_6 is affected by cobalt substitution for magnesium by T_c decreases.

Introduction

It is well known that the lead magnesium tungstate (Pb_2MgWO_6) makes part from complex perovskite compounds with general formula $Pb^{2+}B^{2+}_{1/2}B^{6+}_{1/2}O_3$ in which distribution of the B^{2+} and B^{6+} ions occurs when a large difference exist in either charges or ionic radii [1, 2]. At 38^oC the Pb_2MgWO_6 undergoes a phase transition from the rhombic paraelectric to the tetragonal antiferroelectric phase with a well defined suprastructure [1, 3].

In our previous works we have reported the influence of the Mn, Fe and Cu substitution for Mg on structure, dielectric and magnetic properties of Pb_2MgWO_6 compound [4-6]. It was observed formation of the solid solutions in the large concentration of these substitutions with suprastructure characteristic for these materials [1, 3]. The T_c temperature increases when the substitution of Mg is realized by Mn and Cu [5, 6] and decreases in case of Fe [4].

In order to investigate other solid solutions of this compound, in this work we present the substitution Co for Mg influence on structural and electrical properties of $Pb_2Mg_{1-x}Co_xWO_6$ solid solutions.

Experimental

The polycrystalline samples of $Pb_2Mg_{1-x}Co_xWO_6$ with $0 \le x \le 0.3$ were prepared by reacting stoichiometric proportion of PbO, WO_3, $Mg(NO_3)_2 \cdot H_2O$ and Co_2O_3 chemicals with analytical reagent grade purity. The admixtures

were mechanically homogenized using an agate mortar and calcined at 700^{o}C for 4 hours. After this procedure the samples were mechanically homogenized, pressed in pellets and sintered at 1000^{o}C for 1 hour in air. The pellets have 1–1.5 cm^2 area and 1-3 mm thickness.

The X-ray diffraction measurements were performed on a DRON-2 type equipment using Cu-K_α radiation.

Dielectric permitivity measurements were carried out in the temperature range 20 – 60^{o}C at 1 KHz using Keithley 3300 LCZ-meter. For good electrical contacts, the samples area were silvered with silver paste.

Results and discussion

The X-ray diffraction patterns (Fig. 1) were indexed and show a tetragonal structure for all prepared samples, having cell parameters: a = c = 16·10 Å and b = 15.98 Å for sample with x = 0.01. The most intense diffraction lines are indexed as single perovskite structure and lines of lower intensity as suprastructure reflections. By cobalt substitution for magnesium there is a small increase of lattice parameters, which is probable a consequence of the difference in the ionic radii of Mg^{2+} (0.67 Å) and Co^{2+} (0.73 Å). For x > 0.1 on the diffraction patterns can be observed the weak lines which are not attributed to the basic structure of the solid solutions. Probable our samples contain a small quantities of unidentified structural phase, which not have significant influence on the properties.

The temperature dependence of the dielectric permitivity for $Pb_2Mg_{1-x}Co_xWO_6$ samples is shown in Figure 2. As can be seen dielectric anomaly at T_c (38^{o}C) related to the antiferroelectric transition in Pb_2MgWO_6 is affected by cobalt substitution for magnesium. The Curie temperature decreases with cobalt contents, as was observed also in the case of $Pb_2Mg_{1-x}Fe_xWO_6$ solid solutions [4]. The variation of T_c is a common property for complex systems that involves ferroelectric or antiferroelectric transition [1]. As it is expected the Curie temperature tends to $T_c \cong 32^oC$ [2, 7] which is Curie temperature for Pb_2CoWO_6 compound (o – Fig. 2).

Conclusions

X-ray diffraction and dielectric permitivity measurements performed on $Pb_2Mg_{1-x}Co_xWO_6$ with $0 \le x \le 0.3$ indicate that the solid solutions are formed. The partial cobalt substitution for magnesium determines a small increase of lattice parameters of Pb_2MgWO_6. It was evidenced that the Curie temperature of these solid solutions decreases when the Co concentration increase.

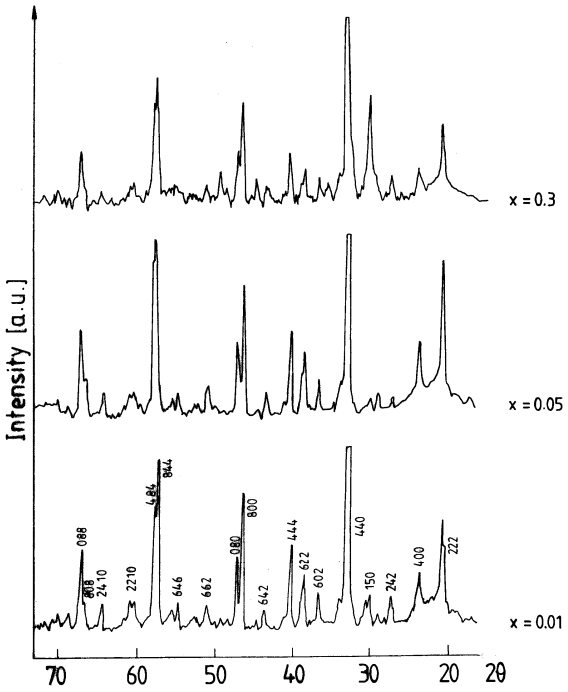

Fig. 1. X-ray diffraction patterns for $Pb_2Mg_{1-x}Co_xWO_6$ solid solutions.

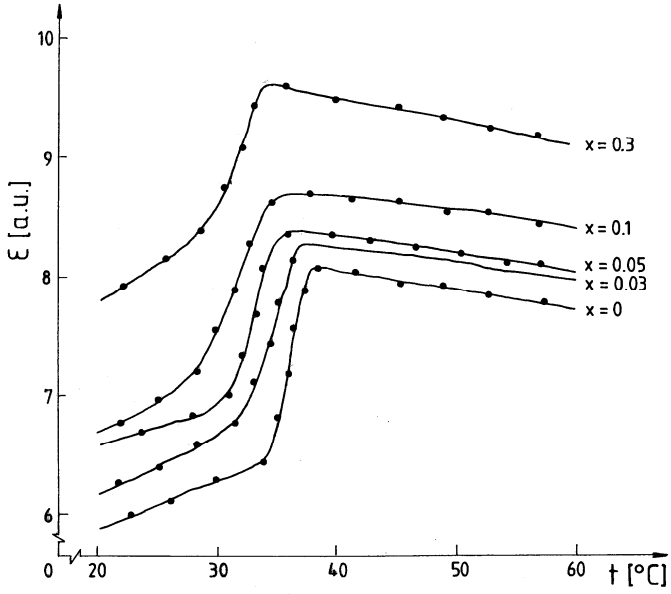

Fig. 2. Temperature dependence of the dielectric permitivity for $Pb_2Mg_{1-x}Co_xWO_6$ solid solutions.

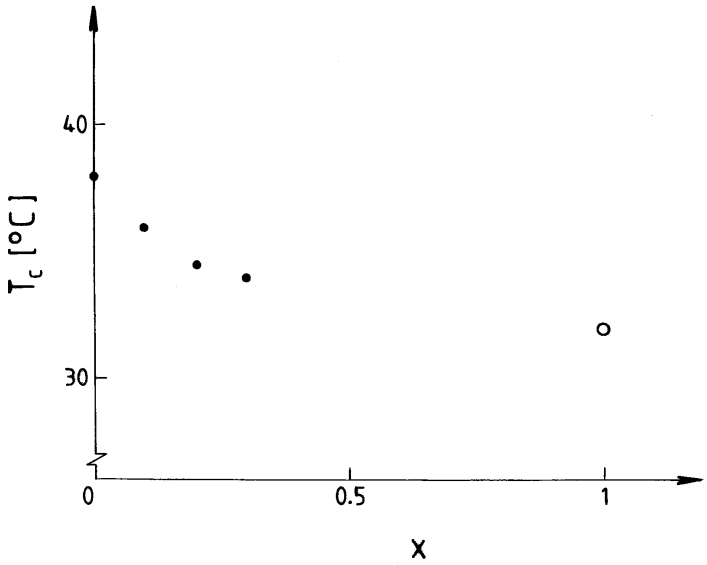

Fig. 3. The composition dependence of T_c for $Pb_2Mg_{1-x}Co_xWO_6$ solid solutions.

REFERENCES

1. F.S.Galasso, Perovskites and High – T_c Superconductors, Gordon and Breach Science Publishers, London, 1990
2. W.K.Choo, H.J.Kim, J.Ho.Yong, H.Lim, J.Y.Lee, J.R.Kwon, C.H.Chun, Jpn. J. Appl. Phys. 32, 4249 (1993)
3. N.Bonin, W.Paciorek, K.J.Schenk, G.Chapuis, Acta. Cryst. B51, 48 (1995)
4. I.Barbur, I.Ardelean, J. Mat. Sci. Lett. 12, 1747 (1993)
5. I.Ardelean, I.Barbur, A.Veres, Gh.Borodi, V.Timar, Balkan. Phys. Lett. 5, 892 (1997)
6. I.Barbur, I.Ardelean, Gh.Borodi, A.Veres, Z.Cete, Mat. Lett. (submitted to publication)
7. V.A.Bokov, S.A.Kijaev, I.E.Mylnikova, A.H.Tutov, Fiz. Tverd. Tela 6(10), 3038 (1964).

STUDIA UNIVERSITATIS BABEŞ-BOLYAI, PHYSICA, XLVII, 2, 2002

ESR STUDY OF SOME IRRADIATED CYTOSTATIC DRUGS

G. DAMIAN

"Babeş-Bolyai" University, Department of Physics, RO-3400 Cluj-Napoca, Romania, e-mail: dgrig@phys.ubbcluj.ro

ABSTRACT. Two cytostatic drugs, Mercaptopurine and Azathioprine, have been investigated by ESR spectroscopy in order to detect if they contain or can easily form stable paramagnetic species following sterilization by ionizing radiation. The absorbed dose of drugs was15 kGy corresponding to an average dose used in the sterilization process ESR measurements proved that both of them contained various stable paramagnetic species after irradiation. The Azathioprine drug exhibited very weak ESR signals before irradiation, having hyperfine splitting constant of 15 G and centered around a spectroscopic factor g_0.=2.007. Some spectroscopic properties and suggestions concerning possible structure of the radicals are discussed in this paper.

Keywords: cytostatic, drugs, γ-irradiation, ESR.

INTRODUCTION

The studies of effects of the high-energy ionizing radiation (gamma rays, electron beams) on the medical devices and drugs or on foods, are increasing due to applications in the medical sterilization and hygienic quality of foods [1,2]. The main advantage of these methods is due to high penetrating power and the very small temperature rise induced.

The sterilization dose (Sterility assurance level (SAL) of 10^{-6}) of pharmaceuticals depends on the initial microbiological spoilage and on the microorganisms radiosensitivity [3]. On account of the destructive nature of ionizing radiation and the difficulty in predicting the radiolytic effects, the study of radio-induced radicals and chemical products in drugs is necessary to determine the feasibility of the radiation treatment and to control it. The regulations about the radiosterilization are permitted in some countries and not in others [4-6], therefore it is necessity to differentiate between irradiated and non-irradiated samples.

Electron spin resonance (ESR), which is a very valuable method for detection of free radicals, can be used to study the radiolysis mechanism [7] or to detection of irradiated drugs [8-10] as already used for foodstuffs irradiated at very low dose (100 Gy).

This paper describe the results of experiments on cytostatic drugs (Mercaptopurine and Azathioprine) by EPR, in order to detect if they contain or can easily form stable paramagnetic species following sterilization by ionizing radiation [11,12].

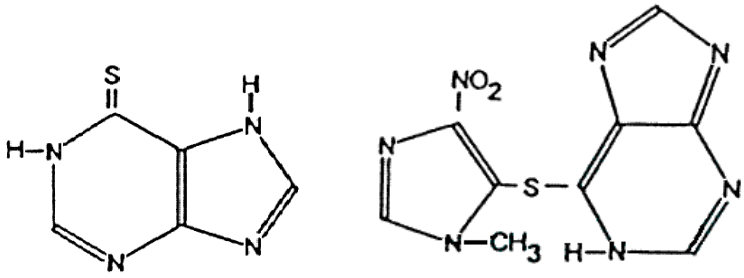

Mercaptopurine Azathioprine

Fig. 1. Structural formula studied compounds

The method has been particularly recommended for unstable substances, i.e. thermolabile or chemically reactive, which can hardly be sterilized thermally or chemically [14,15]. This aspect is especially important for highly bioburden products originating from natural sources [13]. In addition, γ-radiation offers definite advantages such as the possibility of sterilization of drugs in packages and it also ensures a long period of validity. The most important advantage is the possibility of sterilization of thermolabile drugs or those of high chemical reactivity, which are not resistant to other methods of decontamination. One of the most critical points of radiation treatment is the possibility of chemical and physical alterations, which can lead to some undesirable changes, e.g. to a loss of biological activity of the drugs [16].

EXPERIMENTAL

Mercaptopurine and Azathioprine are two compounds from a large series of purine analogues, which interfere with nucleic acid biosynthesis and have been found active against human leukemias [17,18].

Mercaptopurine has the chemical formula, 1,7-dihydro-6H-purine-6-thione, $C_5 H_4 N_4 S xH_2 O$, with molecular weight 170.19, and Azathioprine, as a derivative of mercaptopurin, has the chemical formula 6-[(1-methyl-4-nitro-1H-imidazol-5-yl)thio]-1H-purine, $C_9 H_7 N_7 O_2 S$, with molecular weight 277.26. The structural formulas are presented in Fig. 1.

Mercaptopurine and Azathioprine drugs in the form of microcrystalline powder was exposed to γ-radiation from a ^{60}Co source (GAMMA CHAMBER 900) in ambient conditions. The ^{60}Co source give a compact and uniform density of radiations and a dose debit of 16 Gy/h evaluated by ferrous sulfate dosimetry [19]. The absorbed dose of drugs was15 kGy corresponding to an average dose used in the sterilization process.

Powder samples (non-irradiated and irradiated) were placed in a 20 mm length, 1 mm inside diameter quartz capillary. EPR spectra were recorded at room temperature with a JEOL-JES-3B spectrometer, operating in the X-band

(~9.5 MHz) with a field modulation of 100 KHz, and equipped with a computer acquisition system. The computer simulation analysis of the spectra was made by using a program that is available to the public through the Internet (http://alfred.niehs.nih/LMB) for obtaining the magnetic characteristic parameters.

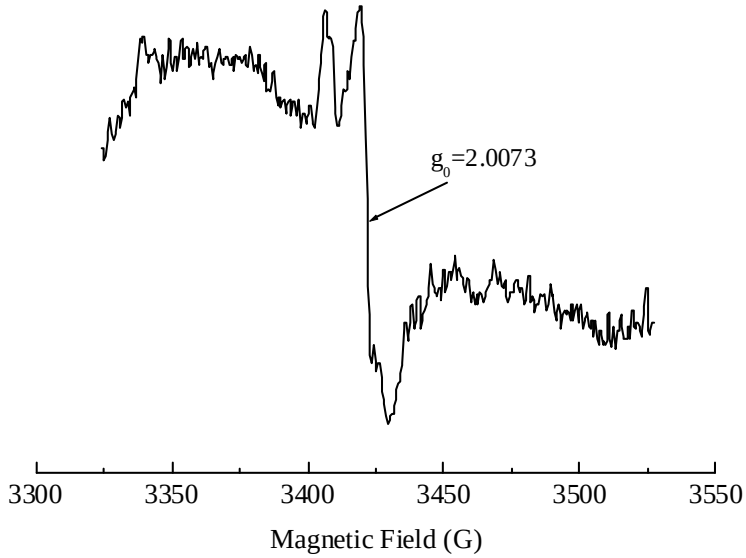

Fig. 2. EPR spectra of non-irradiated Azathioprine

RESULTS AND DISCUSSION

Non-irradiated and irradiated samples were analyzed by EPR spectroscopy. Only non-irradiated polycrystalline sample of Azathioprine exhibit weak EPR signals (Fig. 2) possible, presence of the NO_2 substituent in molecular structure. The detected spectra comprise triplet features which are probably due to hyperfine splitting of nitrogen A_N=15 G and a spectroscopic factor g_0.=2.0073. However that signal cannot be from nitroxyl radicals $R_2NO^{\bullet}$ as these give no detectable signals in condensed media [20]. The populations of the other radicals are very low or not specific and cannot be detected.

By γ-irradiation were generates free radicals detectable for both examined samples.

The spectra consist mostly of broad peaks, which are characteristic for free radicals in the solid state, and cannot be unambiguously identified due to their poor resolution. In Fig. 3 are presented the ESR spectra of irradiated samples at 15 kGy absorbed dose.

The singlet character spectrum of Azathioprine cannot be interpreted, due to low resolution. They exhibit a linewidth of 10.5 G which reflect the random orientations of the radicals with regard to the magnetic and a

broadening mechanisms contribution by dipolar and spin-spin interactions. The total spectrum represents a sum of spectra corresponding to all free radicals simultaneously present in the sample, dominated by a broad central line.

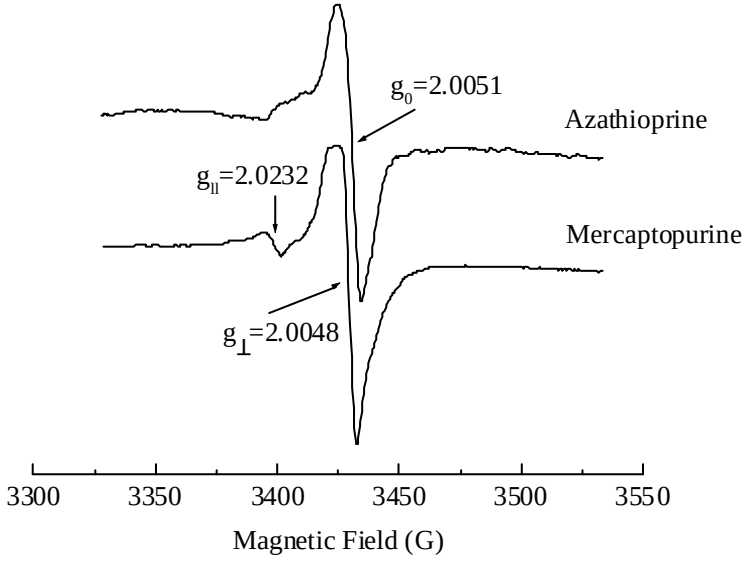

Fig.3. EPR spectra of gamma-irradiated sample at 15 kGy

The broad signal observed was characteristic for free radical trapped in a solid matrix. The value of the isotropic g-factor of g_0=2.0051, is characteristic for carbon - or nitrogen-centered radicals. The unresolved spectrum of Azathioprine does not exhibit any resolution similar to that recorded for the non-irradiated drug. Due to lack of resolution of any hyperfine interaction, the character of the paired radicals cannot be concluded.

The anisotropic spectrum obtained for Mercaptopurine seems to belong to sulphinyl radical $RSO^{\cdot}$ with $g_{||}$ =2.0232 and $g_{\perp}$ =2.0048 formed on oxidation of the thiyl radical [21,22]. This anisotropy in the EPR spectrum, are due probably, the localization of radical centers on both aromatic rings [23] giving rise to a local axial arrangement.

However there is an admixture of other species as can be seen from the spectrum. Thus, the ESR spectrum of polycrystalline powder contains radicals oriented in all possible directions and yields a composite spectrum of lines ranging from $g_{||}$ to $g_{\perp}$.It cannot observe the radical trapped in the drug prior to radiolysis since it is probably at too low a concentration to be seen together with the generated, highly populated radical, manifested as a poorly resolved anisotropic singlet.

CONCLUSIONS

Gamma irradiation gives rise to a free radical species in chemical compounds, and electron paramagnetic resonance (EPR) yields valuable informations on the stability of the drugs in the sterilization process. It was observed that the various substituents of similar compounds, give free radicals species with deferent paramagnetic characteristics. By increasing of molecular structure of drugs, the possibility of existence of free radicals in non-irradiated compounds increase too, due to weak strength bonds of substituted groups. The generations of free radicals is not dramatically for medical treatments; only the possibility of chemical and physical alterations can lead to some undesirable changes, e.g. to a loss of biological activity of the drugs. The formed free radicals in gamma-sterilized medicines dissolved in aqueous solutions cannot exist any longer as free radicals, they converting rapidly into stable nonparamagnetic compounds.

REFERENCES

1. Saint-Lebe, L., Raffi, J., *Cah. Nutri. Diete*., Paris 30 (2), 117-123 (1995)
2. Farkas, J., *Int. J.Microbiol*. 9, 1-45 (1989).
3. Jacobs, G.P.. *Radiat. Phys. Chem*. 26, 133-142 (1985)
4. Pharmacopeia, *Commission des Communautes Europeennes, Bonnes pratiques de fabrication des medicaments; la reglementation des medicaments dans la Communaute Europeenne*, 1992.
5. Pharmacopeia, 1993, *British Pharmacopeia*, Appendix XVIII, A197-A199.
6. Pharmacopeia, 1995, *United States Pharmacopeia*, XXIII, 1976-1981.
7. Crucq, A-S., *Chim. Nouv*. 12, 1356-1359 (1994)
8. Zeegers, F., Crucq, A-S., Gibella, M., Tilquin, B., *J. Chim. Phys*. 90, 1029-1040 (1993)
9. Gibella, M., Crucq, A-S., Tilquin, B., *J. Chim. Phys*. 90, 1041-1053 (1993)
10. Basly, J.P., Longy, I., Bernard, M.,. *Pharmaceutical Research* 14, 810-814(1997)
11. Dam, A.M., Gazso, L.G., Kaewpila, S., Maschek, I., *Radiat. Phys.Chem*. 47, 515 (1996)
12. Varshney, L., Patel, K.M., *Radiat. Phys. Chem*. 43, 471(1994).
13. Byun, M.-W., Yook, H.-S., Kwon, O.-J., Kang, I.-J., *Radiat. Phys. Chem*.49, 483(1997)
14. Jacobs, G.P., Wills, P.A., *Radiat. Phys.Chem*. 31, 685(1988)

15. Phillips, G.O., *Radiation technology in surgery and the pharmaceutical industry: An overview of applications*. IAEA Bulletin 1, 19(1994)
16. Jacobs, G.P., *Radiat. Phys. Chem*. 28, 133(1985)
17. Loo TL, Luce JK, Sullivan MP, Frei E III. *Clin Pharmacol Ther.*;9:180-194(1968)
18. Elion GB. *Fed Proc.*;26:898-904(1967).
19. V.Chi¿, G.Damian, L.David, O.Cozar, V.Znamirovschi, L.Kazimirski, D.Ristoiu, *Studia UBB, Physica*, XLII, 1, 40-48(1997)
20. Symons, M.C.R*., Chemical and biochemical aspects of Electron-Spin Resonance Spectroscopy*. Van Nostrand Reinhold Co, London., 1978.
21. Swarts, S.G., Becker, D., DeBolt, S., Sevilla, M.D,. *J. Phys. Chem*. 93, 155(1989)
22. Sevilla, M.D., Becker, D., Yan, M.., *Int. J. Radiat. Biol*. 57, 65(1990)
23. Ambroz, H.B., Kornacka, E.M., Marciniec, B., Ogrodowczyk, M., Przybytniak, G.K., *Radiation Physics and Chemistry* 58 357-366 (2000)

STUDIA UNIVERSITATIS BABEŞ-BOLYAI, PHYSICA, XLVII, 2, 2002

SURFACE-ENHANCED RAMAN SPECTROSCOPY OF 5-(4 BROM-PHENYL)-FURAN –2 CARBALDEHIDE ON SILVER SOL

T. ILIESCU[a*], F. D. IRIMIE[b], M. BOLBOACA[c], CS. PAIZS[b], I. BRATU[d], R. PACURARIU[a], W. KIEFER[c]

[a] *Babes-Bolyai University, Physics Faculty, 3400 Cluj-Napoca, Romania.*
[b] *Babes-Bolyai University, Chemistry Faculty, 3400 Cluj-Napoca Romania.*
[c] *Institut für Physikaliche Chemie, Universität Würzburg, D-97074,Würzburg, Germany*
[d] *INCDTIM, Cluj-Napoca, Romania*

ABSTRACT. FT-Raman and SER spectra of 5-(4-brom-phenyl)-furan-2 carbaldehide at pH 1 were recorded and analyzed. The absence of carbonyl band in SER spectrum was explained by the hydration of carbonyl bond. The shift by 5-13 cm^{-1} of SERS bands and change in their relative intensity by comparing with ordinary Raman spectrum, indicate the chemisorption of the sample molecules on the silver surface via the nonbonding electrons of the ring oxygen.

Keywords: Raman Spectroscopy, SERS, Furan-2 carbaldehide derivatives.

Introduction

Surface-Enhanced Raman Spectroscopy (SERS) has been applied to a variety of situations. Major applications have been in the development of analytical SERS sensor [1] and in following chemical reactions on surface [2]. The technique has also elucidated much information about the behavior of molecules adsorbed at metal surface [3]. By using of surface selection rules [4,5], the estimation of orientation of molecular species on the surface can be obtained. Long-range classical electromagnetic effects and short-range charge transfer are the two main mechanisms leading to large enhancement of the Raman signal [6,7]. SERS has already been observed for many drugs. In order to know the action of the potential drugs, as our derivative, is very important to study if the structure of adsorbed species is the same as free species. In these studies the silver surface serves as an artificial biological interface [8].

Furan- 2 carbaldehide derivatives are very important intermediates in organic synthesis. The bacteriostatic effects of these compounds were checked up with good results.

In present study, we recorded FT Raman and SER spectra on silver sol of 5-(4-brom-phenyl)-furan-2 carbaldehide (5-(4Br-P)-F-2C) at pH 1 in order to elucidate the adsorption behavior of these molecules on silver surface. To our knowledge these data are not yet present in the literature.

[*] *Corresponding author. E-mail ilitra@phys.ubbcluj.ro*

Experimental

The data about the preparation of furan-2 carbaldehide and FT Raman spectrometer was presented anywhere [9]. SER spectra were recorded with Spex 1404 double spectrometer using 514.5 nm and 300 mW output of Spectra Physics argon ion laser. The detection of Raman signal was carried out with a Photometrics model 9000 CCD camera. Spectral resolution was 2 cm^{-1}. A citrate reduced Ag colloid was employed as SERS substrate. Ag citrate was prepared according to the literature [10]. A small amount of 10 μL of 5-(4Br-P)-F-2C 10^{-1}mol l^{-1} ethyl alcohol solution was added to 3-ml colloid. 0.1 ml 10^{-1}mol l^{-1} NaCl solution was also added for producing a stabilization of the colloidal dispersion and a considerable enhancement of the SER spectra. The final concentration of the sample was approximately 3.2 10^{-4} mol L^{-1}. H_2SO_4 were used to obtain the requested pH value.

Results and discussion

FT-Raman spectrum of solid sample (Ordinary Raman Spectrum (ORS)) and SER spectra in silver sol at pH value 1 are presented in Fig.1a and 1b respectively.

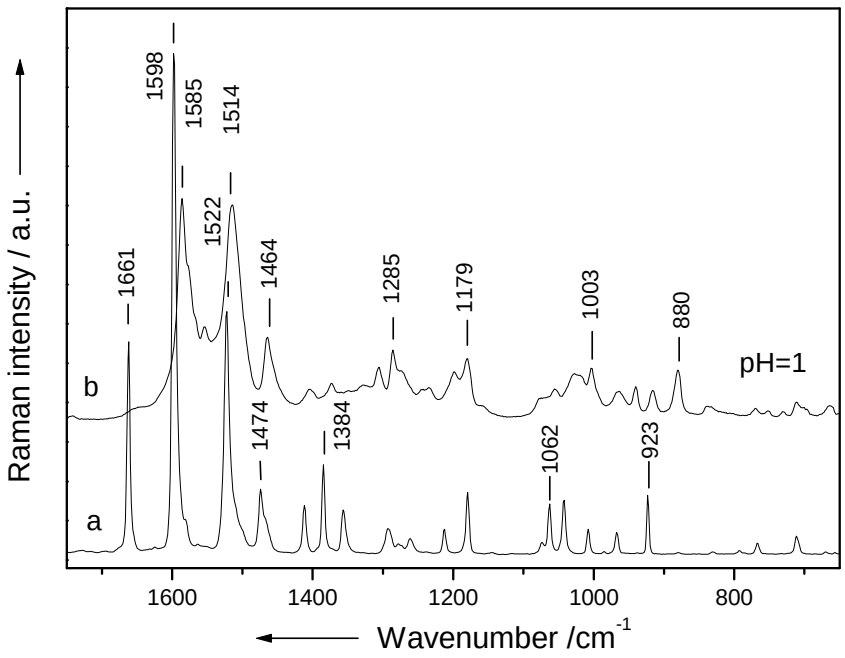

Figure 1. a) FT Raman (solid state) and b) SER spectra of 5-(4 brom-phenyl)-furan-2 carbaldehide in silver sol at pH 1. Concentration of the sample 3.2 10^{-4} mol L^{-1}

We avoided the alkaline value of pH because in this case, according to Cannizzaro reaction there are many species present in solution and analysis of adsorbed species is very difficult.

FT Raman and SERS data are presented in Table 1.

Table 1.

Experimental (FT-Raman) and SER spectrum at pH 1 of 5-(4-brom-phenyl)-furan-2 carbaldehide.

Raman	**SERS pH 1**	**Assignment**
174w		$\delta(C_{1,2,3}) + \delta(C_{4,5,6})$
229w		$\omega(C_{10}C_{11})$
280w		$\delta(CBr) + \delta(C_{4,5,7})$
359vw		ring 1[b] + ring 2[c] out of plane def.
436w		$\delta(C_{5,7,8})$
516w		ring 1 out of plane def.
630m	639(w) 663(w)	$\delta(C_{5,6,1}) + \delta(C_{2,3,4})$
711m	711(w)	$\delta(C_{1,2,3}) + \delta(C_{4,5,6})$
766m	770(w)	$\delta(C_{9,10.11})$
793w		ω(CH) (ring 2)
831w	838(w)	ω(CH) (ring 1)
879vw	880(m)	τ(CH) (ring 2)
923m	916(w) 940(w)	τ(CH) (ring 1)
967m	964(w)	$\delta(C_{9,10}O_1)$
1007m	1003(m)	$\delta(C_{6,1,2}) + \delta(C_{3,4,5})$
1041m	1027(m)	ring 1 breathing
1062m 1073sh	1055(w)	ρ(CH) (ring 1) + $\nu(CBr)$
1179m	1179(m)	δ(CH) (ring 1) + $\nu(C_7O_1C_{10})$
1212m	1198(m) 1242(vw)	ρ(CH) (ring 2)
1278m	1275(w)	$\nu(C_{5,7})$
1293m	1285(m)	ρ(CH) (ring 1)
1356m	1327(vw)	$\nu(C_{8,9}) + \delta$(CH) (COH)
1384m	1372(w)	δ(CH) (COH)
1411m	1404(w)	ring 1 stretching + $\nu(C_{8,9}) + \delta$(CH) (COH)
1474m	1464(m)	ρ(CH) (ring 1) + ring 2 stretching
1506sh 1522s	1514(s)	ring 1 + ring 2 stretching + $\nu(C_{5,7}) + \nu(C_{10,11})$
1583sh 1598vs	1576(sh) 1585(s)	ring 1 + ring 2 stretching
1661s		ν(CO) (COH) anti-form
2859w		ν(CH) (COH)
3058sh 3069m		ν(CH) (ring 1)
3113m 3126sh		ν(CH) (ring 2)

*Abbreviation: w-weak, m-medium, s-strong, v-very, sh-shoulder, ν-stretching, δ-bending, ρ-rocking, τ-twist, ω-wagging,. ring 1[b]-phenyl ring, ring 2[c]-furan ring.

The significant differences between the FT-Raman and SER spectra concerning the relative intensities, bandwidths and peak position indicate an interaction between the metal and adsorbate.

If the molecules are physisorbed on the metal surface, its spectrum is practically the same as that of free molecules, small differences being observed only for the bandwidth [6]. When the molecules are chemisorbed there is an overlapping of the molecular and metal orbitals the molecular structure of adsorbate being modified [7].

Comparing the SER spectrum of 5-(4Br-P)-F-2C to the corresponding ORS (se Fig.1a and 1b) a shift of the peak positions can be observed. Therefore, we conclude that 5-(4Br-P)-F-2C molecules are chemisorbed on the silver surface.

The bands that appear in the 1450-1600 cm^{-1} spectral range are very intense both in ORS and SERS. A shift to lower wavenumber in SER spectrum can be observed from 1598, 1582, 1522, 1474 cm^{-1} to 1585, 1578, 1514, 1464 cm^{-1}. The medium intense bands present in the ORS at 1411, 1384 and 1356 cm^{-1} are very weak and shifted to 1404, 1372 and 1326 cm^{-1} in SER spectrum. The weak bands observed in the 1300-600 cm^{-1} region in ORS have the corresponding shifted band in the SER spectrum.

The bandwidths of the SERS bands at pH 1 are larger than that of the corresponding ORS bands. This broadening can be explained by the interaction between the molecules and silver surface.

By rotation of CHO group 5-(4Br-P)-F-2C presents two, *syn*- and *anti*-form, isomers As a consequence of the interaction with silver surface it is possible that vibrational mode specific to sin-form isomer, which in ORS is not presents, to be active in SERS. Also is possible that bands specific to each isomer to not be resolved after adsorption.

The enhancement of Raman signal in SERS can be explained through two main mechanisms, electromagnetic and chemical one [6,7]. In our case it is very difficult to separate the contribution of these two mechanisms, both contributing to the enhancement of the Raman signal. Additionally, it is possible to have some resonance contribution to the total enhancement because the excitation wavelength 514.5 nm falls in the wing of the absorption band of 5-(4Br-P)-F-2C solution.

Inspection of the Fig.1b and Table 1 shows that the stretching C=O vibration of *anti*-form isomer in SER spectrum at pH 1 is absent, while in ORS appear at 1661 cm^{-1} .

The absence of the band due to the carbonyl stretching mode in SERS at pH 1, can be a consequence of the hydration of the C=O bond. The same situation was observed for formylpiridine [11] and 4 and 2-acetylpiridine [12]

According to the surface selection rules [13], the vibrations of the adsorbed molecules which have a polarizability tensor component parallel to the normal on the metal surface, will be preferentially enhanced compared to the bulk spectrum.

In the SER spectrum of 5-(4Br-P)-F-2C at pH value 1 (Fig.1b) the bands at 1585, 1576 and 1514 cm^{-1} assigned to the ring stretching modes and the band at 1179 cm^{-1} assigned to the in plan bending vibration are more enhanced than other modes and red shifted by 8-13 cm^{-1} by comparison to the ORS spectrum. At this value of the pH the bands due to out of plane deformation of the phenyl and furan rings are practically absent, while the bands at 838 and 916 cm^{-1} given by CH wagging and CH twisting modes (see Table 1) are only weakly enhanced. Therefore, we suppose that molecular planes of adsorbed molecules are vertical or less tilted oriented with respect to the silver surface. The bands at 663, 940, 1242 cm^{-1} present in SER spectrum, have not correspondence in the bulk spectrum and are probably due to the surface complex formed by adsorption.

The small shift and enhancement of the band at 1179 cm^{-1} that involves the vibration of the furan ring oxygen reveals that the interaction between oxygen atom and the metal surface *via* it the lone pair electrons is not so strong.

Conclusions

5-(4-brom-phenyl)-furan-2-carbaldehide presents a good SER spectrum only at low value of the pH. The absence of the carbonyl stretching band in SERS was explained by hydration of C=O bond in the surface adsorption state.

The red shift of the SERS band by comparing to the ordinary Raman spectrum indicate the chemisorption of molecules on the silver surface which are tilted oriented to the metal surface and bonded to it *via* nonbonding electrons of the ring oxygen.

REFERENCES

1. R.L. Garrell, *Anal. Chem.* **61**, (1989) 401 A
2. J. S. Suh, K. H. Michaelian, *J. Phys. Chem.,* **91,** (1987) 598
3. M. Moskovits, J. S. Suh, *J. Phys. Chem.,* **27**, (1988) 3940
4. C. S. Allen, R. P. Van Duyne*, Chem*. *Phys. Lett*., **63,** (1979) 455
5. X. Gao. J. P. Davis, M. J. Weaver, *J. Phys. Chem.,* **94**, (1990) 6858.
6. T. V. Dinh, *Trends in Anal. Chem.*, **17**, (1998) 557
7. ACampion, P. Kambphapati, *Chem. Soc. Rev***., 27**, (1998) 241.
8. G. Dryhusrst, *Electrochemistry of Biological Molecules*, Academic Press, New York, 1977, p. 473.

9. T. Iliescu, F. D. Irimie, M. Bolboaca, Cs. Paizs, W. Kiefer, *Vibr. Spectr.* (2002) in press.
10. T. K. Lee, D. Meisel, *J. Phys. Chem.*, **87**, (1982) 3391
11. K. Mukherjee, D. Bhattacharjee, T. N. Misra, *J. Colloid. Interface Sci*., **193**, (1997) 286
12. K. A. Bunding, M. L. Bell, *Surf. Sci*., **118**, (1983) 329.
13. J. A. Creighton, *Surf. Sci*., **124**, (1983) 209.

STUDIA UNIVERSITATIS BABEŞ-BOLYAI, PHYSICA, XLVII, 2, 2002

STRUCTURE AND VIBRATIONAL FREQUENCIES OF 5-(4 BROM-PHENYL)-FURAN-2 CARBALDEHIDE: DENSITY FUNCTIONAL THEORY STUDIES

T. ILIESCU[a*], F. D. IRIMIE[b], M. BOLBOACA[c], CS. PAIZS[b], I. BRATU[d], R. PACURARIU[a], W. KIEFER[c]

[a] *Babes-Bolyai University, Physics Faculty, 3400 Cluj-Napoca, Romania.*
[b] *Babes-Bolyai University, Chemistry Faculty, 3400 Cluj-Napoca Romania.*
[c] *Institut für Physikaliche Chemie, Universität Würzburg, D-97074,Würzburg, Germany*
[d] *INCDTIM, Cluj-Napoca, Romania*

ABSTRACT. Infrared and FT-Raman 5-(4-brom-phenyl)-furan-2 carbaldehide were recorded and analyzed. Theoretical calculations at the BPW91/6-311+G* levels of theory were performed for the two, *syn*- and *anti*-form rotational isomers. *Anti*-form isomer was found to be more stable than syn-form by 0.795kJ mol^{-1}. Temperature dependence at the intensity corresponding to the C=O stretching vibration confirms the results obtained by theoretical calculations that, anti-form isomer is most stable one. The theoretical ΔH=0.845 kJ mol^{-1} value is close to the experimental ΔH=0.726 kJ mol^{-1} value obtained by temperature dependence of the C=O stretching mode coresponding to the *anti*– and *syn*-form.

Keywords: Raman and IR Spectroscopy, DFT calculation, Furan-2 carbaldehide derivatives.

Introduction

Furan- 2 carbaldehide derivatives are very important intermediates in organic synthesis. The bacteriostatic effects of these compounds were checked up with good results.

The action of many drugs is determined by their structure. In this sense we performed the investigation of two rotational isomers of 5-(4-brom-phenyl)-furan-2 carbaldehide (5-(4Br-P)-F-2C) from an analytical (infrared and Raman spectroscopy) and theoretical (DFT) calculations point of view. To our knowledge these data are not yet present in the literature.

Experimental

The compounds were obtained from the corresponding diassonium salt and furfural in aqueous medium using $CuCl_2$ catalyst. [1] The products were purified with column chromatography on silica gel.

* *Corresponding author. E-mail ilitra@phys.ubbcluj.ro*

The FT Raman spectra were recorded using a Brucker IFS 120HR spectrometer with an integrated FRA 106 Raman module and a resolution of 2 cm^{-1}. Radiation of 1064 nm from Nd-YAG laser was employed for excitation. A Ge detector, cooled with liquid nitrogen, was used. The infrared spectrum in KBr pellet was recorded with a Brucker IFS 25 spectrometer and resolution 2cm^{-1}.Temperature dependence of the IR spectrum was obtained using UR 10 spectrometer. The density functional theory (DFT) calculations were performed using GAUSSIAN98 [2]. All calculation of harmonic wavenumber was performed using a fully optimized geometry as reference geometry. The DFT geometry optimization was carried out with the combination of Becke's 1988 exchange functional [3] and the Perdew-Wang 91 gradient-corrected correlation functional [4] (BPW91). The 6-311+G* basis sets for all atoms has been employed in the geometry optimization and the vibrations calculations.

Results and discussion

The structural formulas of the two rotational isomers of 5-(4Br-P)-F-2C are presented in Fig.1.

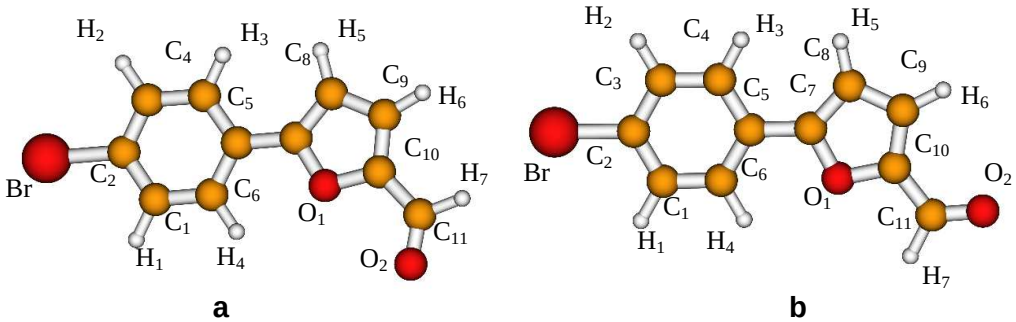

Figure 1. Structural formulas of the two isomers of 5-(4-brom-phenyl)-furan-2 carbaldehide: (a). syn-form, (b) anti-form isomers.

FT-Raman spectrum of solid sample is presented in Fig.2a and calculated Raman spectrum in Fig. 2b.

By rotation of the (CHO) group in the sample, two conformations can be obtained, *syn*-form and *anti*-form rotamer. The optimized geometry of these conformations, obtained at BPW91/6-311+G^* level of theory with the labeling of their atoms is shown in Fig.1. The optimized structure of both conformers is planar. Further, the analytical harmonic modes have been calculated in order to ensure that the optimized structure corresponds to minim on the potential energy surface. The total energy for the *syn*- and *anti*-form isomers, including zero-point corrections, is found to be – 3147.902901 and – 3147.903204 hartree, at the BPW91/6-311+G^* level of theory. Therefore, the *anti*-form isomer was found to be more stable than *syn*- form isomer by 0.795 $kJ.mol^{-1}$.

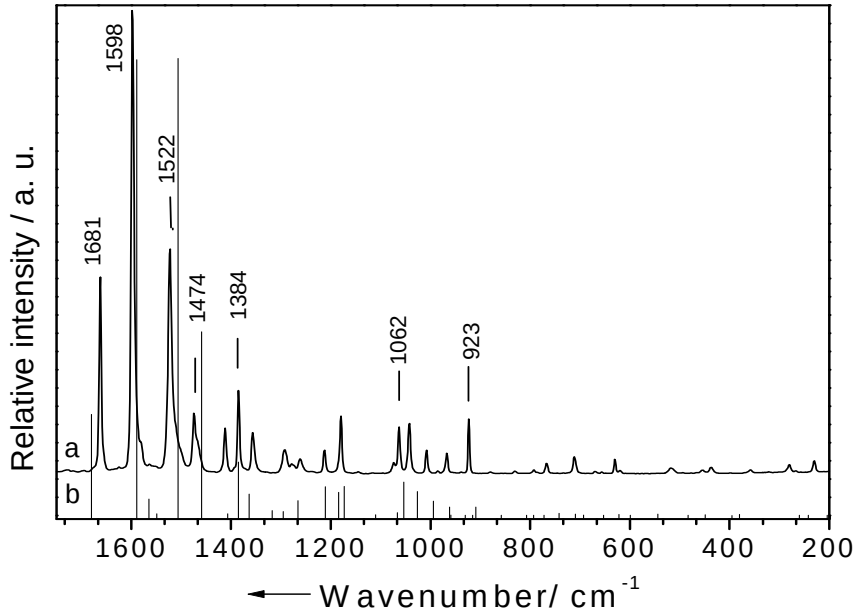

Figure 2. (a). FT-Raman spectrum and (b). the calculated Raman wavenumber of 5-(4-brom-phenyl)-furan-2 carbaldehide.

The observed bands in infrared and FT-Raman of 5-(4Br-P)-F-2C with the calculated wavenumber at BPW91/6-311+G* levels of theory for both isomers are summarized in Table 1. The tentative assignment of vibrational modes is also presented.

Table 1.

Experimental (infrared, FT-Raman) and calculated wavenumbers (cm^{-1}) (anti/syn forms) of 5-(4-brom-phenyl)-furan-2 carbaldehide.

IR	Raman	DFT[1].anti/syn	Assignment
	174w	204/180	$\delta(C_{1,2,3}) + \delta(C_{4,5,6})$
	229w	242/221	$\omega(C_{10}C_{11})$
	280w	260/260	$\delta(CBr) + \delta(C_{4,5,7})$
	359vw	380/418	ring 1[b] + ring 2[c] out of plane def.
437w	436w	449/430	$\delta(C_{5,7,8})$
494m	516w	544/503	ring 1 out of plane def.
628w	630m	622/621	$\delta(C_{5,6,1}) + \delta(C_{2,3,4})$
712m	711m	709/704	$\delta(C_{1,2,3}) + \delta(C_{4,5,6})$
773s	766m	772/766	$\delta(C_{9,10.11})$
793vs	793w	793/805	ω(CH) (ring 2)
831m	831w	807/823	ω(CH) (ring 1)
880vw	879vw	858/850	τ(CH) (ring 2)
923m	923m	930/955	τ(CH) (ring 1)

IR	Raman	DFT[1].anti/syn	Assignment
967s	967m	962/960	$\delta(C_{9,10}O_1)$
1006m	1007m	994/993	$\delta(C_{6,1,2}) + \delta(C_{3,4,5})$
1042s	1041m	1053/1058	ring 1 breathing
1063sh 1073m 1117w	1062m 1073sh	1066/1070	ρ(CH) (ring 1) + ν(CBr)
1170vw	1179m	1184/1188	δ(CH) (ring 1) + $\nu(C_7O_1C_{10})$
1212w 1260m	1212m	1211/1201	ρ(CH) (ring 2)
1278w	1278m	1266/1248	$\nu(C_{5,7})$
1291w	1293m	1295/1292	ρ(CH) (ring 1)
1357w	1356m	1364/1355	$\nu(C_{8,9})$ + δ(CH) (COH)
1385sh	1384m	1385/1391	δ(CH) (COH)
1411m	1411m	1407/1414	ring 1 stretching + $\nu(C_{8,9})$ + δ(CH) (COH)
1475s	1474m	1459/1469	ρ(CH) (ring 1) + ring 2 stretching
1502sh 1522w	1506sh 1522s	1506/1514 1549/1553	ring 1 + ring 2 stretching + $\nu(C_{5,7})$ + $\nu(C_{10,11})$
1597w-m	1583sh 1598vs	1565/1569 1589/1596	ring 1 + ring 2 stretching
1681vs 1695 sh	1661s	1680/1689	ν(CO) (COH) anti-form ν(CO) (COH) syn form
2848w	2859w	2830/2840	ν(CH) (COH)
3060w	3058sh 3069m	3117/3133 3129/3147	ν(CH) (ring 1)
3112w	3113m 3126sh	3140/3157 3144/3160	ν(CH) (ring 2)

*Abbreviation: w-weak, m-medium, s-strong, v-very, sh-shoulder, ν-stretching, δ-bending, ρ-rocking, τ-twist, ω-wagging.
, DFT[1]=BPW91/6-311+G*; ring 1[b]-phenyl ring, ring 2[c]-furan ring.

The assignment of the normal modes of vibration for the molecules was accomplished mainly by comparison with related molecules [5,6] and using wavenumber (unscaled values) and intensities as obtained by the BPW91 method. The theoretical results obtained with the BPW91/6-311+G* basis set reproduce closest the experimental values. A strict comparison between the experimental and calculated wavenumbers and intensities is not possible in this case, because the experimental data were obtained for the solid state whereas the theoretical results are for gas phase. It is well known that the calculated wavenumbers are obtained using the harmonic approximation, whereas the experimental wavenumbers are anharmonic by nature. Nevertheless, as revealed by Fig.2 and Table 1, the quality of the quantum chemical results of the presented theoretical level is sufficient to be useful for the assignment of the experimental data.

The 5-(4Br-P)-F-2C in solid state contain both isomers, identified by the presence of two bands given by the C=O stretching vibration, at 1681

and 1695 cm^{-1} in the infrared spectrum (see Fig. 3) assigned to the *anti*- and *syn*-form respectively. In FT-Raman solid state spectrum only one band is present in this spectral region. The assignment of these bands to the corresponding rotamers was made with the help of theoretical calculation. Thus from these calculations the band at 1680 cm^{-1} is specific to *anti*-form isomer, while the band at 1689 cm^{-1} corresponds to the *syn*-form isomer. Comparing the intensities of these bans from infrared spectrum we assume that the *anti*-form isomer is the preponderant rotamer in the solid state sample. In the FT-Raman spectrum only band assigned to the C=O stretching mode of *anti*-form isomer is Raman active.

Additional information concerning the most stable rotamer can be obtained from temperature variation studies [7]. The spectral region (1600-1700 cm^{-1}) of the C=O stretching vibration in the infrared spectrum of 5-(4Br-P)-F-2C recorded at different temperatures are presented in Fig.3. The intensity of the band 1695 cm^{-1}, specific to the *syn*-form isomer, increases and the intensity of the band 1681 cm^{-1}, specific to anti-form isomer, decreases as the temperature increasing, and confirms the results obtained by theoretical calculation, that *anti*-form is most stable one.

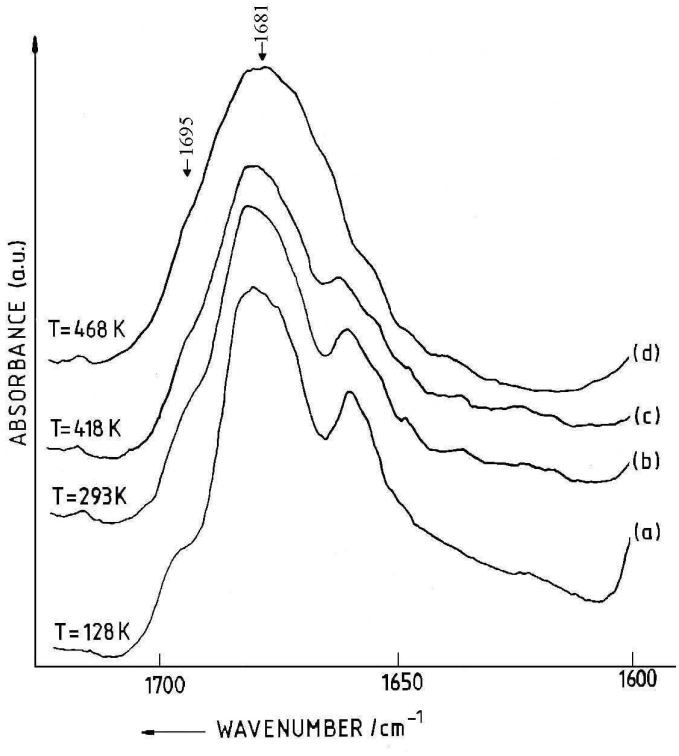

Figure 3. The 1600-1700 cm^{-1} spectral region of infrared spectrum of 5-(4-brom-phenyl)-furan-2 carbaldehide recorded at different temperatures (a). 128 K, (b) 293 K, (c). 418 K, (d) 468 K

From the dependence of logarithmic ratio of the intensities of these bands *vs* 1/T presented in Fig.4, we obtained, according the relation [8]:

$$\ln [I_{1695}/I_{1681}] = - \Delta H/R\ (1/T) + \Delta S/R$$

the value ΔH=0.726 kJ mol^{-1}, close to the value ΔH=0.845 kJ mol^{-1} resulted from theoretical evaluation.

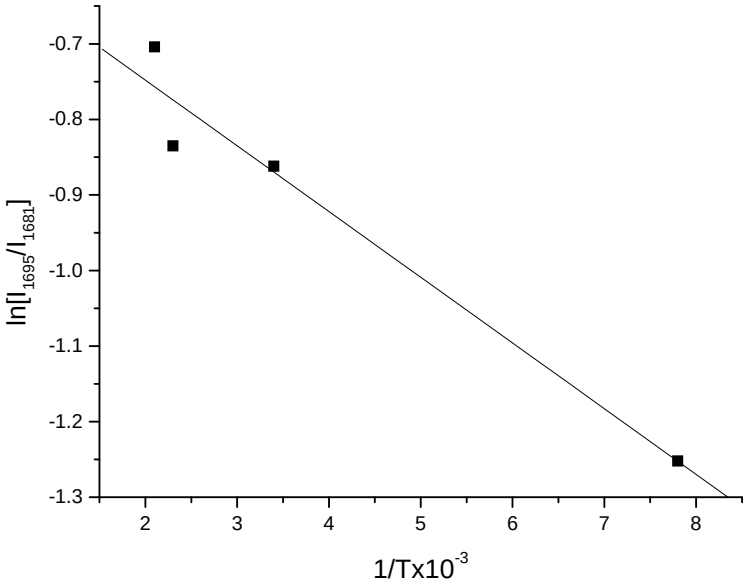

Figure 4. The plot of ln [I_{1695}/I_{1681}] *vs* 1/T

Conclusions

Infrared and FT-Raman spectroscopies were applied to the vibrational characterization of 5-(4-brom-phenyl)-furan-2-carbaldehide. Theoretical calculation at BPW91/6-311+G* levels of theory performed for the two, *syn*-form and *anti*-form rotational isomers, revealed that the *anti*-form isomer is more stable than *syn*-form isomer by 0.795 kJ.mol^{-1}

The assignment of vibrational modes is presented by comparison with related molecules and using wavenumber (unscaled values) and intensities as obtained by the BPW 91 method.

In solid state FT-Raman spectrum of 5-(4-brom-phenyl)-furan-2-carbaldehide only anti-form isomer presents the band due to the stretching of carbonyl bond while in infrared spectrum, both isomers are active in this spectral region.

The experimental ΔH=0.726 kJ mol^{-1} value is close to ΔH=0.845 kJ mol^{-1} obtained by theoretical valuation.

REFERENCES

1. F. D. Irimie, Cs. Paizs, M Tosa, C. Majdik, P. Moldovan, R. Misca, M. Caprioara, *Studia Univ. Babes-Bolyai, Chemia*, **45**, (Nr. 1-2), (2000), 23.
2. Gaussian 98, Revision A7, Gaussian, inc. Pittsburg PA, 1998.
3. A.D. Beeke, *Phys. Rev*. **A38,** (1988), 3098.
4. J. P. Perdew, Y. Wang, *Phys. Rev*., **B45 ,** (1992), 13244.
5. F. R. Dollish, W. G. Fately, F. F. Bently, *Characteristic Raman Frequencies, of Organic Compounds*, John Willey and Sons, New York, !974, p. 220-224.
6. A. R. Katritzky, Ed., *Physical Methods in Heterocyclic Chemistry*, Vol. II, 1963, Academic Press, New York, p. 201-208.
7. G. A. Crowder, F. Northams*, J. Chem. Phys*., **50**, (1969), 4865).
8. B. Schrader, Ed., *Infrared and Raman Spectroscopy Methods and Applications*, Wenheim, New York, 1995, p.687.

STUDIA UNIVERSITATIS BABEŞ-BOLYAI, PHYSICA, XLVII, 2, 2002

INVESTIGATION OF IRRADIATED DRUG INGREDIENTS BY ESR SPECTROSCOPY

G. DAMIAN

"Babeş-Bolyai" University, Department of Physics, RO-3400 Cluj-Napoca, Romania, e-mail: dgrig@phys.ubbcluj.ro

ABSTRACT. The active drug ingredients (amino acids) and inactive drug ingredient (starch), have been investigated by ESR spectroscopy in order to detect stable paramagnetic species following sterilization by gamma radiation. The absorbed dose of drugs was 25 kGy corresponding to the dose used in the sterilization process. ESR measurements proved that studied active ingredients contains various stable paramagnetic species after irradiation. The irradiated samples show large signals, more or less complex, depending on the chemical nature of the amino-acid. Some spectroscopic properties and suggestions concerning possible structure of the radicals are discussed in this paper.

Keywords: excipients, drugs, γ-irradiation, ESR.

INTRODUCTION

In the last two decades, the study of ionizing radiation (gamma rays, electron beams) effects on the medical devices and drugs, has increasing more and more due to applications in the medical sterilization [1,2]. The main advantage of sterilization by ionizing radiation method is due to high penetrating power and the very small temperature rise induced. The method has been particularly recommended for unstable substances, i.e. thermolabile or chemically reactive, which can hardly be sterilized thermally or chemically [3,4]

The studies of different aspects of drug irradiation have been the subject of a systematic research, reported in the literature [5, 7]. The interactions between drug and different forms of energy are very complex and depend on the irradiation and postirradiation conditions. Gamma irradiation can produces changes in the physical and chemical quality of the drugs with the loss the biological activity [3]. However, the presence of free radicals as a radiolytic products [8] is common for all these changes. A number of physical, chemical and biological techniques have been used to detect these changes. From these techniques, ESR is best suited to detect the presence of free radicals due to its high sensitivity to unpaired electrons [9-13]. However, due to the complex nature of the phenomena, correct assignments and characterizations of these radicals are very difficult and, thus, the results given in the literature contain ambiguities.

The aim of this paper is to present the results of on main excipients used in the drugs manufacture by ESR, in order to detect if they contain or can easily form stable paramagnetic species following sterilization by ionizing radiation [11,12]. Drug ingredients are organic compounds or modified simple sugars (starch) used in mixtures with a lot of pharmaceutical products. The role of active ingredients is to stimulate or modulate the translation initiation factors, to transport parthway for poorly permeable drugs or even nutritional complements for some patients [14-17]. The excipients (inactive drug ingredients) have, in general, the role of matrix or protection layer for drugs.

EXPERIMENTAL

Some amino acids and starch in the form of microcrystalline powder was exposed to γ-radiation from a ^{60}Co source (GAMMA CHAMBER 900) in ambient conditions. The ^{60}Co source give a compact and uniform density of radiations and a dose debit of 16 Gy/h evaluated by ferrous sulfate dosimetry [19].

The absorbed dose of ingredients was25 kGy corresponding to absorbed dose used in the sterilization process.

Irradiated powder samples were placed in a 20 mm length, 1 mm inside diameter quartz capillary. ESR spectra were recorded at room temperature with a JEOL-JES-3B spectrometer, operating in the X-band (~9.5 MHz) with a field modulation of 100 KHz, and equipped with a computer acquisition system. The computer simulation analysis of the spectra was made by using a program that is available to the public through the Internet (http://alfred.niehs.nih/LMB) for obtaining the magnetic characteristic parameters.

RESULTS AND DISCUSSION

Amino acids are the basic structural units of proteins. With the exception of proline, amino acids have a common structure. The structure consists of a central carbon atom (alpha carbon), to which is bonded to an amino acid (-NH2), a carboxyl group (-COOH), and a hydrogen atom. Bound to the carbon atom, each amino acid has an additional chemical group, called the R group. The R group is a larger aliphatic side chains and varies from one amino acid to another; diving to each amino acid distinctive properties. Proline also has an aliphatic side chain but it differs form other members of the set of twenty in that its side chain is bonded to both nitrogen and carbon atom resulting a cyclic structure [18]. The structure formulas of studied amino acids are presented in Fig.1.

Starch is a polysaccharide, which is a compound, made from ten or more monosaccharides chemically linked together. A polysaccharide is also called a polymer, which is a large molecule formed when small molecules of the same kind join together to form chains. Starch is made from a chain of sugar molecules. More specifically, starch is a polymer made from a form of glucose called alpha-D-glucose. A molecule of starch can have anywhere from four hundred to several hundred thousand alpha-D-glucose units. The structural formula of glucose unit is represented in Fig. 2.

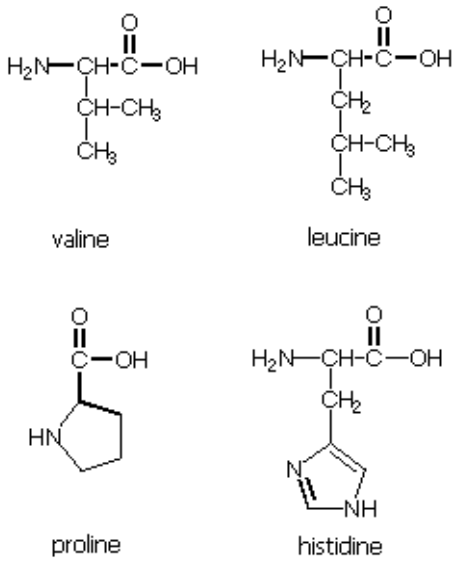

Fig. 1. Structural formulas of studied amino acids

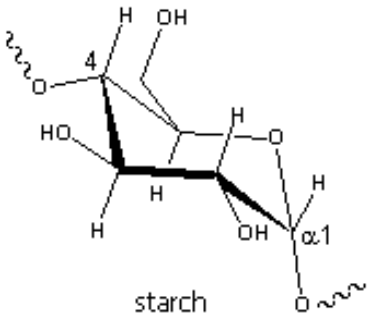

Fig. 2. Structural formula of alpha-D-glucose unit

By γ-irradiation were generates free radicals detectable for all examined samples.The ESR spectra consist mostly of broad peaks, which are characteristic for free radicals in the solid state, and cannot be unambiguously identified due to their poor resolution.

The case of amino-acids (Fig. 3 and Fig.4) seems also simple: the unirradiated samples show no ESR signal, and the irradiated ones show large signals, more or less complex, depending on the chemical nature of the amino-acid. The multiplet lines are characteristic to presences of free radicals in amino acids. The main differences between ESR spectra of irradiated amino acids are due to the structure of aliphatic side chains (R groups), as a result of prevalences ones or other types of free radicals. The main difficulty in the analysis of ESR spectra, is due to the overlapping of different signals in the same magnetic field. However, it can make some assumption about nature of generated free radicals [19, 20] starting from computer simulations of experimental spectra taking in account three species. Table 1 summarizes the important radicals supposedly identified in this study. In general, the symmetrical multiplet lines belonged to the free radicals where the unpaired electrons were localized on carbon atoms. The total spectrum represents a sum of spectra corresponding to all free radicals simultaneously present in the sample, dominated by a broad central line. The broad signal observed was characteristic for free radical trapped in a solid matrix.

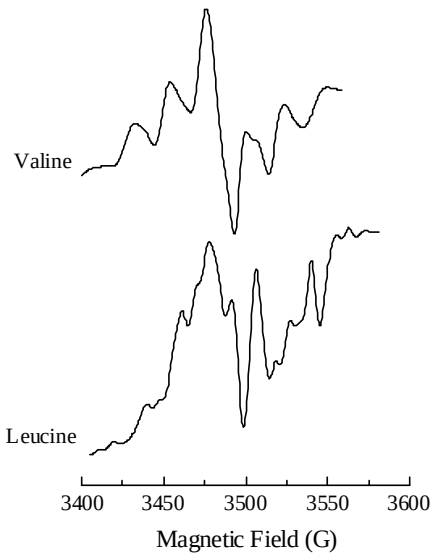

Fig.3. EPR spectra of gamma-irradiated sample of noncyclic amino acids

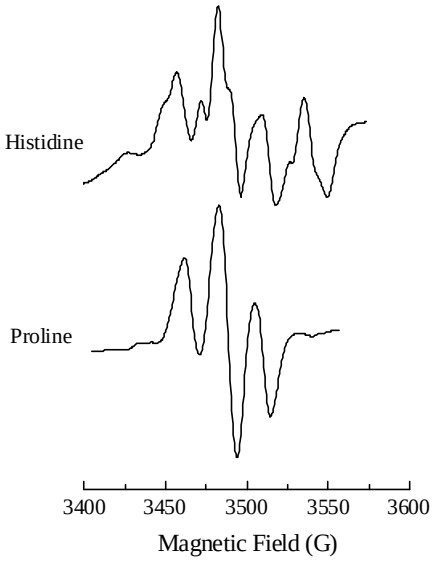

Fig.4. EPR spectra of gamma-irradiated sample of cyclic amino acids

The triplet centered at g=2.0033 with 10.7 G peak-to peak line width for piroline, is due to two equivalent protons with hyperfine coupling a≈20 G which are in very good agreement with the isotropic couplings generally found for carbon centered π radicals. The radical fragment giving rise to this triplet is of the form R-CH_2 that can be produced by removal of a hydrogen atom from the methyl group. The hydrogen abstraction is one of the most commonly mechanisms of producing free radicals in aliphatic compounds containing aromatic rings [21].

Table 1.

The ESR characteristics of free radicals generated in studied aminoacids

Type of radical		Number of lines	ESR parameters
(A)	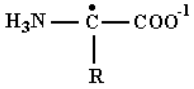	3	g=2.0033, a≈20G
(B)	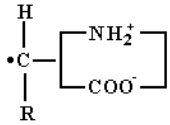	5	g=2.004, a≈22G
(C)	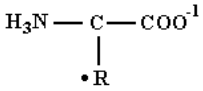	8	g=2.0041, a≈17G

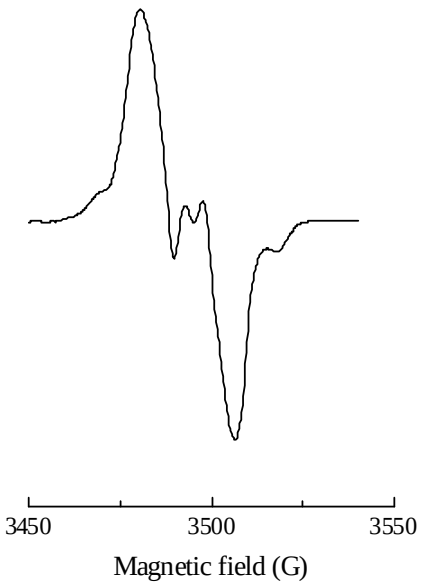

Fig. 5 EPR spectrum of irradiated starch

The characteristic ESR spectrum of irradiated starch, that has been considered as a triplet [22] centered on g=2.0035, though only a pair of lines occurring to the left and right side of the major signal are obvious, looks like a doublet (Fig.5).

The triplet signal with hyperfine splitting of 26.1 G is assigned to radical D and doublet splittings of 30 and 32 G assigned to radicals E (Fig.6).

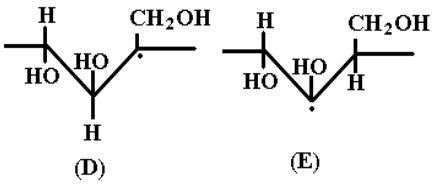

Fig. 6 Proposed types of free radicals generated in irradiated starch

CONCLUSIONS

Gamma irradiation gives rise to a free radical species in chemical compounds, and electron paramagnetic resonance (EPR) yields valuable informations on the stability of the drugs and ingredients in the sterilization process. It was observed that the various substituents of similar compounds, give free radicals species with deferent paramagnetic characteristics. However, the presence of an EPR signal in a complex mixture (ingredients and drugs) make very difficult a rigorous analyses of types of free radicals and its characteristics.This ambiguity is due to the fact that, all organic radicals show EPR signals approximately centered in the same area, 3500 G for 9.5 GHz spectrometers; and that, in solid phase, the EPR spectra are quite always poorly resolved, due to the overlapping of the different spectra relative to the different directions of initial spins with regard to the magnetic field.

REFERENCES

1. L.Saint-Lebe, J.Raffi, *Cah. Nutri. Diete*., Paris 30 (2), 117-123 (1995)
2. J. Farkas, *Int. J.Microbiol*. 9, 1-45 (1989).
3. G.P.Jacobs, P.A.Wills, *Radiat. Phys.Chem*. 31, 685(1988)

4. G.O.Phillips, *Radiation technology in surgery and the pharmaceutical industry: An overview of applications*. IAEA Bulletin 1, 19(1994)
5. G.P.Jacobs, *Radiat. Phys. Chem*. 26, 133-142 (1985)
6. P. Piccerelle, J.-P. Reynier, J. Joachim, B. Tilquin, J.Raffi, *J. Pharma. Belg*. 55 (2000)131–136.
7. H. Ambroz, E. Kornacka, B. Marciniec, M.Ogrodowczyk, G. Przybytniak, *Radiat. Phys. Chem.* 58 (2000) 357–366.
8. A-S. Crucq, *Chim. Nouv*. 12, 1356-1359 (1994)
9. F.Zeegers, A-S. Crucq, M.. Gibella, B. Tilquin, *J. Chim. Phys*. 90, 1029-1040 (1993)
10. M.Gibella, A-S. Crucq, B. Tilquin, *J. Chim. Phys*. 90, 1041-1053 (1993)
11. J.P.Basly, I. Longy, M. Bernard, *Pharmaceutical Research* 14, 810-814(1997)
12. A.M. Dam, L.G. Gazso, S. Kaewpila, I. Maschek, *Radiat. Phys. Chem*. 47, 515 (1996)
13. L.Varshney, K.M. Patel, *Radiat. Phys. Chem*. 43, 471(1994).
14. O.J. Shah, D.A. Antonetti, S.R. Kimball, L.S. Jefferson, *J. Biol. Chem*. 274, 36168–36175 (1999).
15. T.G. Anthony, J.C. Anthony, F. Yoshizawa, S.R. Kimball, L.S. Jefferson, *J. Nutrition* 131 1171–1176 (2001).
16. Z. Todorovic, M. Prostran, S. Vuckocic, *Pharmacol. Res*. 43 (2001) 321–327.
17. K. Hariganesh, J. Prathiba, *J. Pharm. Pharmacol*. 52 1519–1522 (2000).
18. B. Linda, D. M., Eldra Solomon, C. Villee, *Biology.* Third Edition. New York: Saunders College Publishing, 1993.
19. S.Y.Pshezhetskii, A.G. Kotov, V.K.Milinchuk,V.A.Roginskii, V.I. Tupikov, *EPR of free radicals in radiation chemistry*.Halsted Press,New York, 1972.
20. T. Henriksen, T.B. Mela,G.Saxebel, *Free radical in Biology*.Vol.2, Academic Press, London, 1976.
21. M.D.Sevilla, C.Van Paemel, G.Zorman, *J.Phys.Chem*., 76, 3577 (1972)
22. J. Raffi, *ESR identification of irradiated foodstuffs: LARQUA research*. In: McMurray, C.H., Stewart, E.M.,Gray, R., Pearce, J. (Eds.), *Detection Methods for Irradiation Foods*. The Royal Society of Chemistry, Cambridge, U.K, 93 (1996).

STUDIA UNIVERSITATIS BABEŞ-BOLYAI, PHYSICA, XLVII, 2, 2002

INVESTIGATION OF MOLECULAR MOBILITY OF SPIN LABELS IN BSA

G. DAMIAN

"Babeş-Bolyai" University, Department of Physics, RO-3400 Cluj-Napoca, Romania
e-mail: dgrig@phys.ubbcluj.ro

ABSTRACT. EPR spectroscopy was used to study the interaction unsaturated spin label 3-carbamoyl-2,2,5,5-tetramethyl-3-pyrolin-1-yloxy (Tempyo) and bovine serum albumin molecules and bovine serum albumin (BSA). The EPR spectrum of the spin label in the low lyophilized state, exhibits two spectral parts: the major part has a line shape typical for slow isotropic rotational motion, and the minor part typical for faster isotropic rotational fluctuations. The minor parts have a rotational correlation time of $3\text{-}4\cdot10^{-9}$ s, which must be regarded as fast rotation and indicate that these spin adducts are located in flexible nonpolar protein chains, probably at the surface of the protein and the major parts of the spectra have correlation times of $1.8\text{-}2.0\cdot10^{-8}$ s, as result of strong interaction of spin label with polar proteins sites or located inside the globular protein. Quantification by integration of the spectrum yielded ~20 % of the spin label with fast motion and ~80 % with slow motion.

Keywords: EPR spectroscopy, spin label, bovine serum albumin (BSA)

INTRODUCTION

Proteins are polymeric chains that are built from monomers called amino acids. All structural and functional properties of proteins derive from the chemical properties of the polypeptide chain. There are four levels of protein structural organization: primary, secondary, tertiary, and quaternary. Primary structure is defined as the linear sequence of amino acids in a polypeptide chain. The secondary structure refers to certain regular geometric figures of the chain. Tertiary structure results from long-range contacts within the chain. The quaternary structure is the organization of protein subunits, or two or more independent polypeptide chains.

Examination of the amino acid sequence of proteins shows no obvious pattern of hydrophobic and hydrophilic amino acids, but in the tertiary structure of proteins almost all the hydrophobic sidechains are found in the interior of the protein and almost all hydrophilic sidechains are found on the outside of the protein, interacting with water. Most proteins can be characterized as globular (ball-like) with a well defined external surface and a well defined internal core. Just as in micelles, the exterior to be polar and the interior to

be non-polar. Charged residues are amino acids that have charged sidechains are seldom buried in the interior of a folded protein. They are normally found on the surface of the protein where they interact with water and with other important biological molecules. Note that these groups can be important in the recognition (binding) of oppositely charged groups on molecules that interact with proteins [1].

The ionizable groups on the side-chains of charged amino acids are often involved in biochemical transactions (binding, catalysis). Therefore, pH usually has rather dramatic effects on the function of proteins. Polar Residues are both buried as well as on the surface of the protein. They either form hydrogen bonds with other polar residues in the protein or with water. Nonpolar residues do not interact with favorably with water. The central core of most proteins is composed almost exclusively of nonpolar residues, stabilized by numerous van der Waals interactions. However, a significant number of nonpolar residues are also found on the surface of the protein. Therefore, it is important to study the interactions of proteins with well defined molecules that will confer the total molecules sufficient affinity for the binding site of interest on protein.

Bovine Serum Albumin (BSA), the most abundant serum protein, has a total of 35 cysteine residues with 17 disulfide bridges, and one free thiol group allowing to interact with a vast array of chemically diverse compounds at specific binding sites [2].

Useful informations related to the interaction between the nitroxide group and the active site of the proteins, can be obtain by EPR spectroscopy using nitroxide radicals (spin labels).

The EPR of nitroxide spin labeled biological molecules have been extensively used in the last decades for the study of their interactions, mobility and microenvironment in biological systems [3,4]. Spin labels are free radicals which can attach themselves to particular sites in biological systems and produce spectra which provide information on changes in the chemical and physical characteristics in the neighborhood of the site [5,6]. The paramagnetic center of a spin label has its unpaired electron on the NO group of a nitroxyl compound. The unpaired electron shown on the lower oxygen, spends time on and strongly interacts with the $I = 1$ nuclear spin of the nitrogen atom to produce a 3-line hyperfine spectrum. When the solvent has a low viscosity (flows very freely) the radical tumbles rapidly to average out the anisotropies, and a spectrum of three narrow lines is obtained. At lower temperatures the viscosity increases and the solvent materials flows very slowly so the nitrogen radical can no longer tumble rapidly, and a smeared out spectrum is produced.

When the spin label attaches itself to a particular site in a biological molecule its spectrum reveals the extent to which free motion or very restricted motion occurs at the site.

In this paper, the interaction between unsaturated nitroxide radical 3-carbamoyl-2,2,5,5-tetramethyl-3-pyrolin-1-yloxy (Tempyo) and bovine serum albumin was studied by EPR spectroscopy.

MATERIALS AND METHODS

Powder samples of bovine serum albumin (SIGMA Chemicals) were used without further purification. Proteins were hydrated in phosphate buffered physiological saline at a final concentration of 10^{-3} M TEMPYO spin label (SIGMA Chemicals) was added to the liquid samples of each protein in a final concentration of 10^{-3} M (protein/spin label molar ratio 1:1) and the pH values were adjusted at optimal value of pH=8.5, corresponding its normal configuration in the environment

The amount of 5 ml from each samples was lyophilized at -5^{o}C for different time intervals and used for the EPR measurements.

EPR spectra for both, liquid and lyophilized samples, were recorded at room temperature with a JEOL-JES-3B spectrometer, operating in the X-band (9.5 GHz), equipped with a computer acquisition system. Samples were placed in quartz (Pyrex) capillary tubes. The spectrometer settings were: modulation frequency 100 kHz, field modulation 1 G, microwave power 20mW.

The computer simulation analysis of the spectra, for obtaining the magnetic characteristic parameters, was made by using a program that is available to the public through the Internet (http://alfred.niehs.nih/LMB).

The lineshape of an EPR spectrum depends, among other factors, on the orientation of the paramagnetic center with respect to the applied magnetic field. In a powder, or a frozen aqueous solution, the paramagnetic centers will be fixed with a random distribution of orientations, and in the case of anisotropic g- and hyperfine interactions this will lead to a broadened EPR spectrum since all orientations contribute equally. In the liquid state, however, the paramagnetic centers are not fixed but undergo rotational fluctuation. In the case of fast rotation, the anisotropic interactions are thereby averaged to zero, giving rise to sharp EPR lines. If the velocity of the rotational motion decreases, the EPR spectrum will approach that of the powder spectrum. Therefore, a rotational correlation time for a paramagnetic molecule can also be determined by EPR using semiempirical formulae [9].

For isotropic motion in the rapid tumbling limit, the spectra will be isotropic with the averages of the principal components of the g-values and hyperfine splitting factor, a^N. The rate of the isotropic motion determines the relative widths of resonances and the width, ΔH_m, of an individual (hyperfine) line, in the first approximation can be written as a function of the z component of the nitrogen nuclear spin number (m=-1, 0, 1) [6, 8]:

$$\Delta H_m = A + B \cdot m + C \cdot m^2 \quad (1)$$

where the A coefficient includes other contributions than motion. The terms B and C are functions related to the rotational correlational time τ for the motion and can be defined as a function of peak to peak line width of the central line, ΔH_0 [G], and the amplitudes of the m-th line I_m [7]:

$$B = \frac{1}{2}\Delta H_0\left(\sqrt{\frac{I_0}{I_1}} - \sqrt{\frac{I_0}{I_{-1}}}\right) = 0.103\omega_e[\Delta g\Delta a^N + 3(\delta g)(\delta a^N)]\tau_B[1+\frac{3}{4}(1+\omega_e^2\tau_B^2)^{-1}] \quad (2)$$

$$C = \frac{1}{2}\Delta H_0\left(\sqrt{\frac{I_0}{I_1}} + \sqrt{\frac{I_0}{I_{-1}}} - 2\right) = 1.181\cdot 10^6[(\Delta a^N)^2 + 3(\delta a^N)^2]\tau_c[1-\frac{3}{8}(1+\omega_e^2\tau_c^2)^{-1} - \frac{1}{8}(1+\omega_e^2\tau_c^2)^{-1}] \quad (3)$$

in which

$$\Delta a^N = a_{zz}^N - \frac{1}{2}(a_{xx}^N + a_{yy}^N), \delta a^N = \frac{1}{2}(a_{xx}^N - a_{yy}^N) \quad (4)$$

$$\Delta g = g_{zz} - \frac{1}{2}(g_{xx} - g_{yy}), \delta g = \frac{1}{2}(g_{xx} - g_{yy}) \quad (5)$$

and $\omega_N = 8.8\cdot 10^{-6} < a^N >$, a^N is the isotropic hyperfine splitting and ω_e the ESR spectrometer frequency in angular units.

In range from $5\cdot 10^{-11}$ to 10^{-9} s (motion in the rapid tumbling limit) and magnetic field above 3300 G, Δg and Δa^N vanish, and the correlation times τ_B and τ_C are directly related to the B and C coefficients by the following simple relations [6]:

$$\tau_B = \tau_z = K_1 \cdot B \quad (6)$$

$$\tau_C = \tau_{x,y} = K_2 \cdot C \quad (7)$$

where $K_1 = 1.27\cdot 10^{-9}$ and $K_2 = 1.19\cdot 10^{-9}$. The average correlation times is:

$$\tau = (\tau_B \cdot \tau_C)^{\frac{1}{2}} \quad (8)$$

The slow motion of spin probe, lead to a broadening of the EPR lines. In this case, the rotational correlation time, τ, is larger than 10^{-9} s, and thus, the Formula 8 is not applicable. The isotropic nitrogen hyperfine splitting changes to a powder like spectrum, with the peak-to-peak distance between the external peaks of the spectrum ($2\cdot a'_{zz}(N)$) depending on the magnitude of the rotational correlation time, τ. Another lineshape theory for slow isotropic Brownian rotational diffusion of spin-labeled proteins has been developed by J. Freed [10]. Thus, the correlation time can be evaluated from the ratio of the observed splitting between the derivate extrema a'_{zz} and principal value a_{zz}, determinated from rigid matrix spectrum [6,8]:

$$\tau = \alpha\left(1 - \frac{a'_{zz}}{a_{zz}}\right)^{\beta} \quad (9)$$

The α and β parameters depend on the kind of the diffusion process. where a and b are empirical constants, which are tabulated in e.g. Poole and Farach, 1987 [9]. For small spin probe, the intermediate jump diffusion is preferable [9].

RESULTS AND DISCUSSION

BSA was chosen as a model for study of molecular interaction spin label located in a globular protein and the partition between proteins phase and surrounding aqueous medium.

In the low concentration liquid state BSA solution, the Tempyo spin label which is a relatively small molecule, gives raise to a spectrum with narrow lines and constant hyperfine splitting, typical for fast isotropic rotational motion (Fig.1) with very low rate of migration between BSA molecule and water. For this kind of rotation, the rotational correlation time can be estimated from the intensity ratio of the low-field and high-field N-lines using a semi-empirical formulas (6-8). For the Tempyo spin label in BSA aqueous solution, the rotational correlation times is $2 \cdot 10^{-10}$ s, which is consistent with fast rotation as expected for a small molecule.

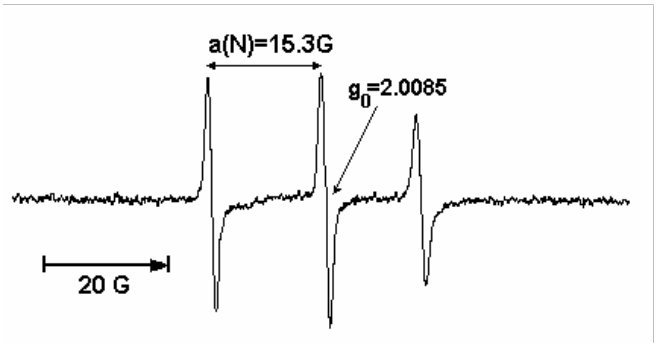

Fig. 1. EPR spectrum of Tempyo in low concentration BSA aqeous solution

When the rate of probe migration is slow on the EPR time scale (~$5 \cdot 10^6$ s^{-1}) and the concentration of probe in the two media is sufficiently high, two distinct subspectra contribute to the observed spectrum. If the rates of probe rotation in the two media are quite different, it is possible to obtain spectra in which resonances due to the probe in two environments are distinguishable (Fig. 2). The ESR spectra of nitroxide spin label in BSA molecules, consist of two spectral parts; the major part marked with arrows, (Fig.2-subspectrum I) has a line shape resembling the powder spectrum of the rigid matrix (strong lyophilized sample-Fig.3) and is typical for slow isotropic rotational motion, and the minor part of the spin label spectrum (marked with an asterisk) is typical for faster isotropic rotational fluctuations (Fig.2-subspectrum II).

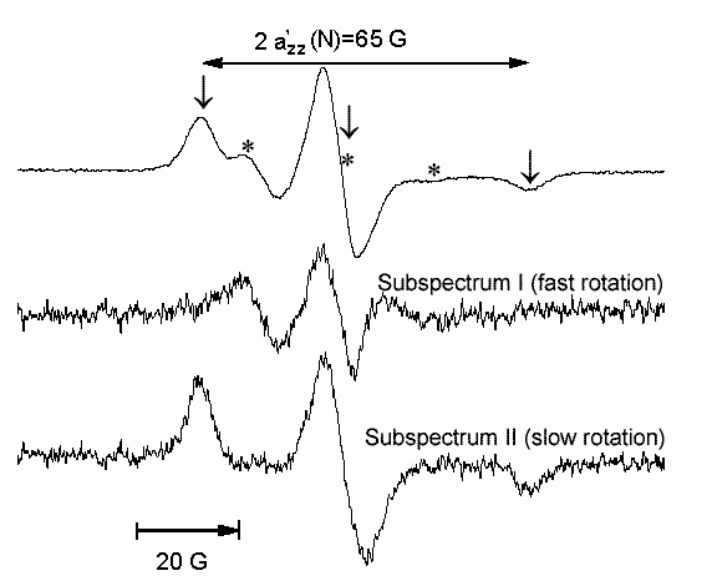

Fig.2. Integral and partially EPR spectrum of Tempyo spin label at high concentration BSA

By comparison of the apparent nitrogen hyperfine splitting (termed $a'_{zz}(N)$) with the nitrogen hyperfine splitting obtained from the rigid matrix spectrum ($a_{zz}(N)$), which are indicated in Fig.2 and Fig.3, the rotational correlation times can be calculated. For an EPR spectrum of a spin label undergoing Brownian rotational diffusion with a linewidths of 3 G, $\alpha=5.4\cdot10^{-10}$ and $\beta= -1.36$.

With the procedures described above the correlation times for isotropics and anisotropics spectra were calculated. The minor parts (marked with an asterisk in Figures 3-7 and 3-8) have a rotational correlation time of $\tau_f = 4.5\cdot10^{-9}$ s, which must be regarded as fast rotation and indicate that these spin label are located in flexible protein chains, probably at the surface of the protein. The major parts of the spectra have correlation times of $1.4\cdot10^{-8}$ s typical for slow rotation and show that The spin labels are located in non-flexible, e.g. folded, parts of the protein.

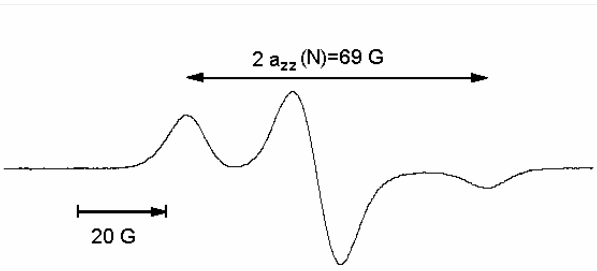

Fig.3. EPR spectra of of Tempyo-BSA at strong lyophylized state

Quantitation of the relative intensities of the two components, by using either spectral subtraction or spectral simulation via the exchange-coupled two-component Bloch equations, yields information on the stoichiometry and specificity of the lipid-protein interaction. Quantification by integration of the spectrum yielded ~20 % of the spin adduct with fast motion and ~80 % with slow motion. By subtracting the minor part (Figure 2-subspectrul I), from the original spectrum (Figure 2-upper spectrum), only the major part remains (Figure 2-subspectrum II). This spectrum implies an almost rigid attachment of the spin label to the globular protein.

The individual spectral components display a lifetime broadening which is determined by the relative populations of the two components and the rate of exchange between them. The exchange rate is determined from τ_f^{-1}, which is the first-order rate constant for exchange from the fluid protein component. The corresponding first-order rate for exchange from the protein-interacting component, τ_b^{-1}, is related to that for the fluid (non rigid) component by mass balance [12]:

$$\tau_b^{-1} = \tau_f^{-1} \cdot \frac{1-f}{f} \tag{10}$$

where f is the fraction of the motionally restricted (protein-interacting) component. Using fraction of the motionally restricted of f=0.8 and correlation time $\tau_f = 4.5 \cdot 10^{-9}$ s, the calculated value off-rate of on BSA is $\tau_b^{-1} = 5 \cdot 10^7 s^{-1}$ corresponding to a slow exchange rate which show no selectivity between adsorption sites of proteins.

CONCLUSIONS

The analysis of the EPR lineshape of the non covalent spin label bovine serum albumine give valuable informations about the dynamic properties (rotational motion) of the nitroxide radical in deferent sites of proteins. Quantitation of the relative intensities of the two components, by using spectral subtraction or spectral, yielded information on the stoichiometry and specificity of the lipid-protein interaction. We have shown that the nitroxide radicals are localized predominantly in folded regions of protein exhibiting EPR spectra typical for slow isotropic rotational motion. The individual spectral components display a lifetime broadening which is determined by the relative populations of the two components and the rate of exchange between them. Such, the calculated exchange rate show no selectivity between adsorption sites of proteins.

REFERENCES

[1] Creighton, T. E. (1983) in Proteins: Structures and Molecular Properties, W.H. Freeman and Company, New York.

[2] Foster, J.R., in Albumin structure, Function and Uses, Rosenoer, V.M., Oratz, M., Rothschild, M.A., Eds., Pergamon, Oxford (1977), p.53-84.

[3] Morrisett, J.D., Wien, R.W., McConnell, H.M. (1973), Ann. N.Y. Acad. Sci. (1973), 222, 149-162.

[4] Jost, P., Griffith, O.H. (1972) in Methods in Pharmacology, Chignell C. Ed., Appleton, New York (1972), p.223-276.

[5] Morrisett, J.D., Pownall, H.J., Gotto, A.M., J.Biol.Chem. (1975), 250, 2487-2494.

[6] Morrisett, J.D. in Spin Labelling – Theory and application, Berliner J. Ed., Acad. Press, (1975) pp. 273-331

[7] Schreier, S., Polnaszek, C.F, Smith, I.C., Biochim. Biophys. Acta, 515, 395(1979).

[8] Goldman, S.A., Bruno, G.V., Polnaszek, C.F., Freed, J.H., J.Chem.Phys., 56,716(1972).

[9] Poole, C. P., Jr., and Farach, H. A. (1987) in Theory of Magnetic Resonance, John Wiley & Sons, New York, NY, pp 319-321

[10] Berliner, L. J. (1976) Spin Labeling, Theory and Application, Adademic Press, New York, NY

[11]. D.E. Budil, K.A. Earle and J.H. Freed, J.Phys.Chem. 97, 1294(1993)

[12] Marsh D (1985). ESR spin label studies of lipid-protein interactions. In: Watts A & De Pont JJHHM (Editors), Progress in Protein- Lipid Interactions. Elsevier, Amsterdam.

STUDIA UNIVERSITATIS BABEŞ-BOLYAI, PHYSICA, XLVII, 2, 2002

INTERMOLECULAR INTERACTIONS IN ORGANIC LIQUIDS

A. CIUPE*, I. LENART*

** Faculty of Physics, "Babes-Bolyai" University, Cluj-Napoca, Romania*

ABSTRACT. An extrapolation of the van der Waals equation of state to the liquid phase by considering the total internal pressure and the dependence of the constants "a" and "b" on temperature and density is made. The validity of the state equation was checked by comparing the values of the ultrasound propagation velocities calculated by these equations to the experimental ones. Based on the state equations the total potential energy of intermolecular interactions, that of dispersion and that of rejection were estimated at different temperatures. The studied liquids were: benzene and carbon tetrachloride in the range 20 – 70^0 C, acetone and chloroform in the range 20 – 50^0C and carbon disulphide in the range 20 – 40^0C.

Introduction

The correlation of the molecular acoustic results with the attempts to establish a state equation for the liquid phase is based on the molecular mechanisms of the ultrasound propagation in the matter. In this respect it has to be emphasized the ultrasound propagation velocity as an acoustic parameter, which by its dependence on the internal energy, on the pressure and the density, may be a verifying tool for the proposed equation.

Hence, in the case of extending the validity of van der Waals' state equation of real gases to the liquid state by introducing some corrections and by solving the proposed equation with respect to the ultrasound propagation velocity, the comparison of calculated values to the experimental ones allows to estimate the validity of this extrapolation.

Theory

To verify the validity of van der Waals' state equation in the case of liquids, Kudreavtev [1], based on the definition of adiabatic sound propagation velocity:

$$c_S^2 = \gamma\left(\frac{\partial p}{\partial \rho}\right)_T \tag{1}$$

by assuming the van der Waals' constants "a" and "b" as independent on temperature, got for it the following formula:

$$c_S = \sqrt{\frac{1}{M}\gamma\left(RT\frac{V^2}{(V-b)^2} - \frac{2a}{V}\right)}. \tag{2}$$

Here: $\gamma = \frac{C_P}{C_V}$, C_p and C_V are the molar heats at constant pressure, respectively at constant volume, p is the pressure, ρ is the density, M is the molar mass, V is the volume, T is the absolute temperature and R is the general constant of gases.

The values of ultrasound propagation velocity calculated by this relation show significant deviations from experimental data. These deviations decrease with increasing temperature, with the tendency of concordance settling only in the range of critical temperature.

W. Schaaffs [2] takes into account the temperature and the density dependence of constants “a” and “b” in the van der Waals’ state equation. He arrives, after some approximations, to the following formula for the ultrasonic propagation velocity:

$$c_S = \sqrt{\gamma \frac{RT}{\rho} \cdot \frac{2b - V}{(V-b)^2}} \tag{3}$$

which leads to values in better agreement with the experimental data.

In the two mentioned attempts the internal pressure is considered in the van der Waals’ formulation in which the intermolecular interactions are limited to those of dispersion. This limitation can explain the observed lake of agreement with the experimental data.

In the present work instead of classical van der Waals’ equation:

$$\left(p + \frac{a}{V^2}\right)(V-b) = RT \tag{4}$$

(where $\frac{a}{V^2} = p_{iw}$) the real internal pressure p_i is introduced and the density dependence of p_i and of b is taken into account. The state equation becomes:

$$[p + p_i(\rho)] \cdot [V - b(\rho)] = RT\,. \tag{4'}$$

Based on this equation (4’), definition (1) leads to the following formula for the ultrasonic propagation velocity:

$$c_S = \sqrt{\gamma \left[RT \frac{\frac{V^2}{M} + \left(\frac{\partial b}{\partial \rho}\right)_T}{(V-b)^2} - \left(\frac{\partial p_i}{\partial \rho}\right)_T \right]}\,. \tag{5}$$

From thermodynamic arguments basis, neglecting external pressure, one obtains a relation for the real internal pressure [3]:

$$p_i = \frac{\alpha T}{\beta_T} = \frac{\alpha T}{\gamma \beta_S} = \frac{\alpha}{\gamma} T \rho c_S^2 \tag{6}$$

where: α is the coefficient of thermal expansion at constant pressure, β_T and β_S are the isothermal and adiabatic compressibility coefficient respectively.

The state equation (4') can be written in the form:

$$\left(p + \frac{\alpha}{\gamma} \rho T c_S^2 \right) \left[V - b(\rho) \right] = RT \,. \tag{4''}$$

In order to express the van der Waals' internal pressure as a function of ultrasound propagation velocity, we used the relation [3]:

$$c_S^2 = \left(\frac{\partial p}{\partial \rho} \right)_S = -\gamma \frac{V^2}{M} \left(\frac{\partial p}{\partial V} \right)_T \tag{7}$$

whence:

$$\frac{M c_S^2}{\gamma V^2} dV = -dp \,. \tag{8}$$

Neglecting external pressure compared with the internal one it results [4]:

$$\int_{V_1}^{V_2} \frac{M c_S^2}{\gamma V^2} dV = \frac{a_1}{V_1^2} - \frac{a_2}{V_2^2} \,. \tag{9}$$

In order to calculate the integral, owing to the unknown dependency of the ultrasound velocity on the molar volume, some approximations have to be introduced. Thus for small V variations we obtain the van der Waals' internal pressure formula:

$$p_{iW} = \frac{1}{2\gamma} \rho c_S^2 = \frac{1}{2\gamma \beta_S} \,. \tag{10}$$

From (6) and (10) we got:

$$p_i = 2\alpha T p_{iW} \tag{11}$$

where $2\alpha T$ represents the correction coefficient of the van der Waals' internal pressure. Hence, the constant "a" in the van der Waals' equation has to be replaced by the corrected constant a_c:

$$a_c = 2\alpha T a \,. \tag{12}$$

Based on state equations (4) and (4') the values of covolume b, respectively $b(\rho)$ can be calculated with formulas:

$$b = V - \frac{RT}{p + p_{iW}} \tag{13}$$

and

$$b(\rho) = V - \frac{RT}{p + p_i}. \tag{14}$$

For non polar liquids the potential energy of interaction by the dispersion forces taken into account in the van der Waals' state equation is:

$$E_{pW} = E_{pdispersion} = -\frac{a}{V}. \tag{15}$$

This energy can be evaluated from van der Waals' internal pressure p_{iW} and the molar volume. Knowing that:

$$p_{iW} = \frac{a}{V^2} \tag{16}$$

it results:

$$E_{pW} = -p_{iW} V. \tag{17}$$

Taking into account formulas (10) and (15), the total potential energy corresponding to all types of interactions is given by relation:

$$E_{ptotal} = E_{pW}\, 2\alpha T = -2\alpha T \frac{a}{V}. \tag{18}$$

Assuming that the aditivity of energies is respected it results:

$$E_{ptotal} = E_{pdispersion} + E_{prejection}. \tag{19}$$

The difference of potential energies defined by relations (15) and (18) gives the potential energy corresponding to the interactions not taken into account by van der Waals' equation, mainly that by rejection forces:

$$\Delta E_p = E_{ptotal} - E_{pdispersion} = E_{prejection}. \tag{19'}$$

RESULTS

Based on the presented relations the ultrasound propagation velocity was calculated using formulas (2) and (5) for: benzene (C_6H_6), carbon tetrachloride (CCl_4), carbon disulfide (CS_2), chloroform ($CHCl_3$) and acetone ($CO(CH_3)_2$) in the temperature ranges: 20 – 70^{0}C for the first two, 20 – 40^{0}C for CS_2 and 20 – 50^{0}C for the two latest substances. The obtained results are presented in table 1, which contains also our experimental measured values of ultrasound propagation velocity and density as well as that of internal pressure p_{iW}, calculated by formula (10) and p_i by formula (11).

For the calculation of γ the following relation was used:

$$\gamma = 1 + \frac{M\alpha^2 c_S^2 T}{C_P} \tag{20}$$

the values of α and C_P being taken from the literature [5].

Table 1

Physical properties of tasted liquids

Liquid	T ^{0}C	ρ kg/m^3	p_{iw} 10^{-5} N/m^2 from (10)	p_i 10^{-5} N/m^2 from (11)	c_{calc} m/s from (2)	from (5)	c_{exp} m/s	$\left(\frac{\partial p_i}{\partial \rho}\right)_T$ x 10^{-5} Nm/kg
C_6H_6	20	879,5	5230	3748	3817	1348	1324	9,0
	30	869,5	4859	3659	3499	1287	1276	8,7
	40	859,3	4518	3568	3210	1205	1231	8,5
	50	846,8	4199	3475	2951	1120	1182	7,5
	60	835,0	3912	3393	2722	1104	1134	7,2
	70	823,0	3641	3305	2498	1085	1086	7,0
CCl_4	2030	1473,0	4804	3463	2964	977	977	4,9
	40	1454,5	4429	3357	2700	950	945	4,8
	50	1436,0	4101	3264	2432	912	915	4,7
	60	1418,4	3788	3163	2262	869	885	4,6
	70	1400,0	3580	3107	2119	831	854	4,5
		1382,0	3239	2977	1892	804	821	4,5
CS_2	20	1264,0	5472	3823	2703	1165	1158	5,1
	30	1248,8	5096	3751	2492	1133	1124	5,0
	40	1233,6	4732	3670	2087	1098	1091	4,9
$CHCl_3$	20	1489,0	4928	3657	1915	986	1001	4,1
	30	1470,5	4551	3587	1864	951	966	4,1
	40	1452,0	4186	3507	1816	916	932	4,0
	50	1431,3	3861	3425	1767	886	898	4,0
$CO(CH_3)_2$	20	790,6	4068	3414	2710	1164	1189	9,8
	30	779,0	3718	3304	2441	1144	1145	8,6
	40	767,4	3414	3213	2211	1108	1102	8,4
	50	755,4	3119	3103	1987	1061	1059	8,0

The tabulated data reflect a good agreement between velocity values calculated based on the real internal pressure values (eq. 5) and the experimental ones. Also it can be observed a significant deviation from experimental data in the case of calculated ultrasound velocities based on the van der Waals' internal pressure (eq.2).

Table 2 contains the calculated values for the internal pressure constants a (eq. 10 and 4) respectively a_c (eq. 12) as well as those for covolumes b (eq. 13) and $b(\rho)$ (eq. 14). The $(\partial b / \partial \rho)_T$ values were calculated from graphical dependence $b = b(\rho)$.

The temperature dependence of potential energy of intermolecular interaction corresponding to the real internal pressure, respectively that corresponding to the van der Waals' internal pressure are presented in fig. 1, respectively in fig. 2 for the five studied liquids.

The difference ΔE_p of potential energies corresponding to the rejection forces varies with temperature as shown by curves in fig. 3. A general presentation of potential energies is illustrated in fig. 4 for benzene.

DISCUTIONS

The state equation (4''), which includes the ultrasound propagation velocity as state parameter, is characterised by a grater volume of structural information compared to the van der Waals classical one.

Table 2

Values of constants "a" and "b"

Liquid	t ^0C	a .10^{-6} $Nm^4/kmol^2$	a_c .10^{-6} $Nm^4/kmol^2$	b .10^3 $m^3/kmol$	b(ρ).10^3 $m^3/kmol$	$\left(\frac{\partial b}{\partial \rho}\right)_T 10^4$ kg/kmol
C_6H_6	20	4,13	2,93	84,15	82,31	-0,63
	30	3,93	2,94	84,64	82,94	-0,65
	40	3,74	2,91	85,14	83,60	-0,67
	50	3,57	2,92	85,89	84,51	-0,72
	60	3,42	2,93	86,46	85,38	-0,73
	70	3,26	2,93	87,07	86,28	-0,75
CCl_4	2030	4,48	3,22	99,82	97,36	-0,47
	40	4,23	3,17	100,05	98,23	-0,48
	50	4,02	3,17	100,75	9912	-0,49
	60	3,81	3,16	101,31	99,91	-0,50
	70	3,61	3,17	102,11	100,83	-0,51
		3,43	3,15	102,48	101,70	-0,51
CS_2	20	1,99	1,38	53,40	51,48	-0,22
	30	1,89	1,39	53,61	51,84	-0,23
	40	1,80	1,39	53,38	52,19	-0,23
$CHCl_3$	20	3,19	2,36	75,22	73,50	-0,34
	30	3,02	2,38	75,64	74,15	-0,35
	40	2,85	2,38	75,99	74,78	-0,36
	50	2,70	2,39	76,44	75,56	-0,37
$CO(CH_3)_2$	20	2,18	1,83	67,43	66,29	-0,52
	30	2,05	1,83	67,74	66,89	-0,54
	40	1,94	1,83	68,02	67,54	-0,55
	50	1,83	1,82	68,24	68,20	-0,56

The satisfactory concordance of theoretical values of propagation velocities, resulted from the acoustical state equation (4''), compared to the experimental data can be explained by the fact that in the corrected state equation all intermolecular interactions in the liquid are comprised, unlike to their limitation to that of dispersion ones in the van der waals' formulation of the state equation.

As concerning the evaluation made for the potential energy of intermolecular interaction, only the dispersion and the rejection forces are considered, this approximation being permitted in the case of studied liquids with the view to their non polar character (excepting the case of chloroform).

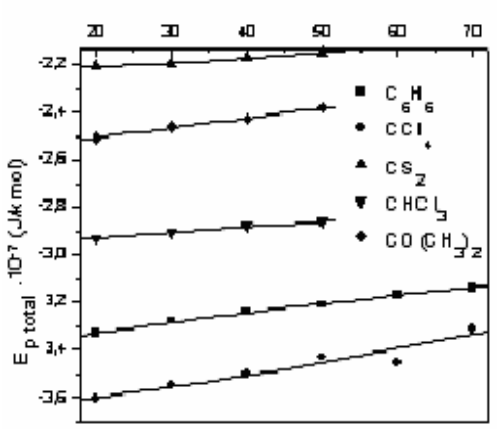

fig. 1

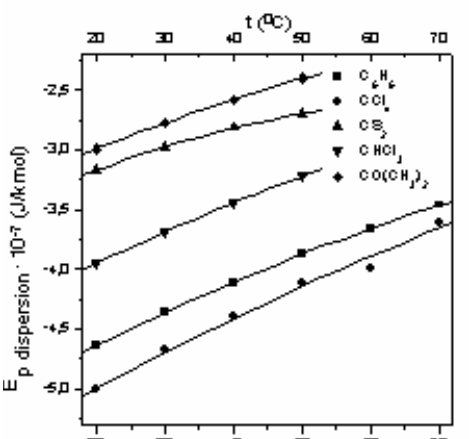

fig. 2

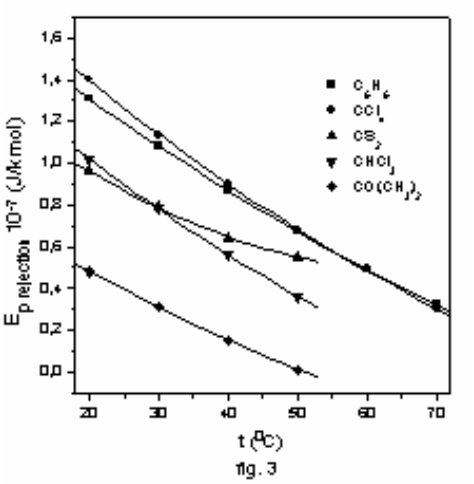

fig. 3

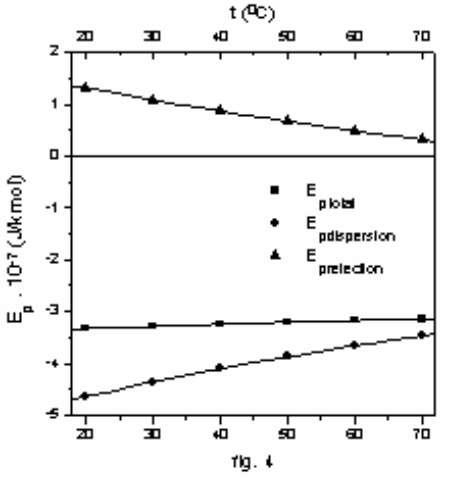

fig. 4

The temperature dependence of interaction potential energies presented in fig. 1, 2, 3 and 4 suits in the first approximation with the dependence of potential energy on the intermolecular distances. The above mentioned approximation results from the not taking into account of nonlinearity of intermolecular distance – temperature dependence. This latest is a consequence of the thermal expansion coefficient rise with increasing temperature.

The taking into account of all intermolecular interactions in the liquid affects also the values of constants a and b in the state equation. Hence, the constant a_c (eq.12) is characterised [3] with a good approximation by independence on temperature; here $a_c < a$.

The coefficient $2\alpha T \to 1$ with temperature increase so that for some characteristic temperature for each liquid, the potential energy of interaction to become negligible, in accordance with conditions in the van der Waals' classical state equation.

The real value of covolume, $b(\rho) < b$, results from the condensed state of the liquids, fact which motivates the considering of the potential energy of rejection.

CONCLUSIONS

The obtained data for the studied liquids show that the corrections introduced to extend the validity of classical van der Waals' state equation to the liquid state, lead to results in better agreement with the experimental data compared to those obtained from alternatives proposed by the other authors [1,2].

Regarding the potential energy of intermolecular interaction, based on the proposed modified equation (4') and using the connection existing between p_i and p_{iW}, it is possible to separate the contribution of attraction forces from that of rejection ones to the global potential energy.

REFERENCES

[1] Kudreavtev B.B., Primenenie ultrakusticheskih metodov v praktike fizikohimiceskih issledovanii, Mopi, Moskva, 1952

[2] Schaaffs W., Molekularakustik, Berlin, 1963

[3] Ausländer D., Lenard I., Ciupe A., Contributions to the Ultrasonic Study of the Internal Pressure of Liquids, Acustica (Stuttgart), 81, p.75, 1995

[4] Melkonean L.G., Scorost' ultrazvuca I mejmolecularnoe pritiajenie v binarnih jidkih smesiah obrazuiuscih himicescoe soedinenie, in the volume Primenenie Ultrazvuk k Issledovanie Vescestvo, red. V.F. Nozdrev, B.B. Kudreavtev, Mopi, Moskva, 1956

[5] Tablitz fiziceskih velicin, Moskva, Atomizdat, 1976 (red. I.K. Kikoin), p. 130 and p. 155

STUDIA UNIVERSITATIS BABEŞ-BOLYAI, PHYSICA, XLVII, 2, 2002

MAGNETIC SUSCEPTIBILITY INVESTIGATION OF IRON IONS IN $3B_2O_3 \cdot KCl$ GLASS MATRIX

I. ARDELEAN and P. PĂŞCUȚĂ

Faculty of Physics, Babes-Bolyai University, 3400 Cluj-Napoca, Romania

ABSTRACT. Magnetic susceptibility measurements have been performed on $xFe_2O_3 \cdot (100-x)[3B_2O_3 \cdot KCl]$ glasses with $0<x\leq20$ mol %. Magnetic data suggest that for $x>5$ mol % the iron ions experience negative magnetic superexchange interactions. From Curie constant values we have established that in these glasses both Fe^{3+} and Fe^{2+} ions are present. The molar fraction of these ions increase with Fe_2O_3 content. Valence states and distribution in glass matrix of iron ions determine the magnetic behaviour of the studied glasses.

1. Introduction

Magnetic susceptibility measurements revealed as very useful to determine the valence states of transition metal ions and the type the interactions involving them over various composition ranges. Their magnetic properties depend on the concentration of the 3d element and the valence states ratio [1-3] as well as on the structure of the vitreoux matrix and implicitly on the conditions of sample preparation [4, 5]. The magnetic behaviour of the oxide glasses containg iron ions was most frequently attributed to an antiferromagnetic coupling within the pairs Fe^{3+}-Fe^{3+}, Fe^{3+}-Fe^{2+} and Fe^{2+}-Fe^{2+} [4, 6, 7].

An antiferromagnetic coupling between iron ions was reported in borate [8, 9], phosphate [7, 10], tellurite [11, 12] and lead-bismuthate [13] oxide glasses.

This work aim to present our results obtained by means of magnetic susceptibility measurements performed on $3B_2O_3 \cdot KCl$ glass matrix gradually doped with Fe_2O_3.

2. Experimental

We have studied $xFe_2O_3 \cdot (100-x)[3B_2O_3 \cdot KCl]$ glasses with $0<x\leq20$ mol % using pure reagent grade Fe_2O_3 , H_3BO_3, and KCl. The mixtures, in suitable proportions corresponding to the desired concentration of Fe_2O_3, were mechanically homogenized and melted in sintered corundum crucibles in an electric furnace at 1200 ˚C. The molten material was kept at this temperature for 30 min, then quenched at room temperature by pouring onto a stainless-steel plate.

The structure of samples was analyzed by means of X-ray diffraction. The pattern obtained did not reveal any crystalline phase in the samples up to 20 mol%. For higher concentration in glasses was evidenced the crystalline microprecipitates.

The magnetic susceptibility measurements were performed using a Faraday-type balance, in the 80-300 K temperature range.

3. Results and Discussion

The temperature dependence of the reciprocal magnetic susceptibility of some glasses from studied system is presented in Figure 1. For the samples with x≤5 mol % a Curie law is observed suggesting that in this concentration range are predominant iron ions which do not participate to the superexchange interactions. For x>5 mol % the reciprocal magnetic susceptibility obeys a Curie-Weiss behavior with a negative paramagnetic Curie temperature (θ_p), characteristic to antiferromagnetic coupling of magnetic ions. The peculiar structure specific to vitreous oxide solids impose the short-range character of magnetic interaction and enhance the structural image of clusters such that the magnetic behavior of the glasses can be described by the mictomagnetic type order [14].

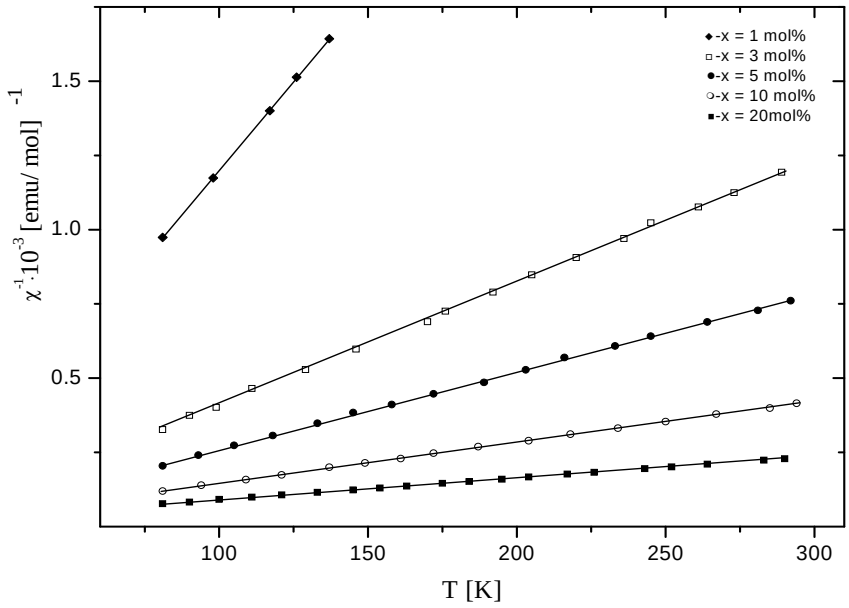

Fig 1. The temperature dependence of the reciprocal magnetic susceptibility for $xFe_2O_3 \cdot (100-x)[3B_2O_3 \cdot KCl]$ glasses with 1≤ x ≤ 20mol%.

The composition dependence of the paramagnetic Curie temperature is given in Figure 2. The absolute magnitude of θ_p values increases for x>5 mol %. The exchange integral increases as the content of the magnetic ions is increased in the glass [15] and as a result the magnitude of the θ_p increases.

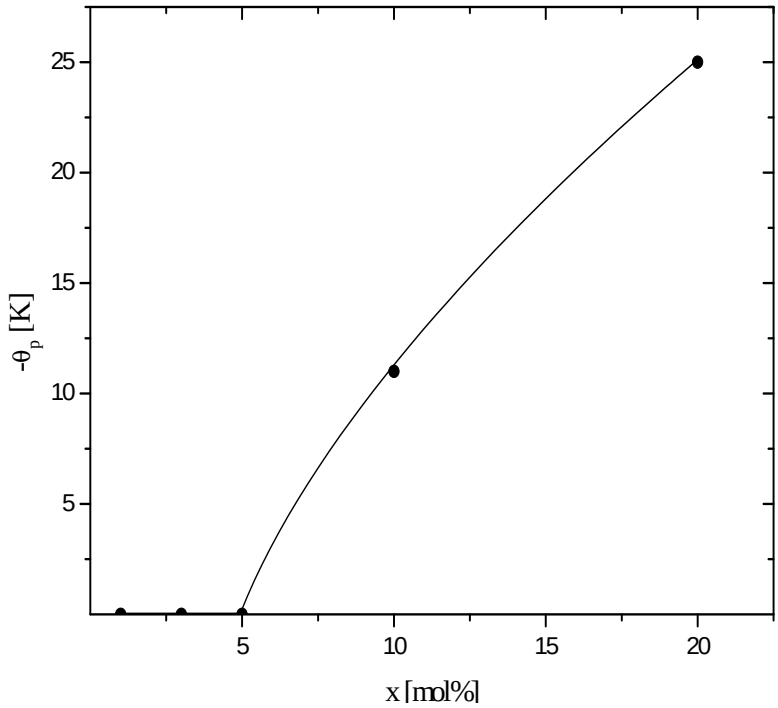

Fig 2. The composition dependence of the paramagnetic Curie temperature for $xFe_2O_3·(100-x)[3B_2O_3·KCl]$ glasses.

The composition dependence of the molar Curie constant (C_M) and effective magnetic moment (μ_{eff}) are presented in Table 1. For all the glasses with the experimental values obtained for molar Curie constant and consequently for effective magnetic moments are lower than those which correspond to the Fe_2O_3 content, considering that all iron ions are in Fe^{3+} valence state, but they are higher than those calculated for the case when all iron ions would be Fe^{2+} species (Table 1). Therefore we consider that in these glasses are present both Fe^{3+} and Fe^{2+} ions. The presence of Fe^{3+} and Fe^{2+} ions has been evidenced in other oxide glasses [1, 5, 8, 10-13]. Having in view this supposition and using the atomic magnetic moment values of free Fe^{3+} and Fe^{2+} ions: $\mu_{Fe^{3+}}$ =5.92μ_B and $\mu_{Fe^{2+}}$ =4.90μ_B [16], we can estimate in first approximation the molar fraction of these ions in the investigated glasses using the relations:

$$x \cdot \mu_{eff}^2 = x_1 \cdot \mu_{Fe^{3+}}^2 + x_2 \cdot \mu_{Fe^{2+}}^2 \quad (1)$$

and

$$x = x_1 + x_2 ,$$

where $\mu_{eff} = 2.827\sqrt{C_M/2x}$ are the experimental magnetic moment, x_1 and x_2 are the molar fraction of iron ions in Fe^{3+} and Fe^{2+} valence states. The results are presented in Table 1. From these data one remarks that the molar fraction of both Fe^{3+} and Fe^{2+} ions increases in whole studies concentration range, last being higher for x>5 mol %.

We have also estimated the ratio

$$r = N_{Fe}^{3+} / N_{Fe}^{3+} + N_{Fe}^{2+} = x_2 / x. \quad (2)$$

This ratio decreases with Fe_2O_3 content from 0.8 for 1 mol % to 0.33 for 20 mol % (Table 1).

Table 1.

Molar Curie constant, C_M, effective magnetic moment, μ_{eff}, molar fraction of $Fe^{3+}(x_1)$ and $Fe^{2+}(x_2)$ ions and the ratio r of Fe^{3+} ions relative to all iron ions contained in $xFe_2O_3 \cdot (100-x)[3B_2O_3 \cdot KCl]$ glasses.

x [mol% Fe_2O_3]	C_M [emu/ mol]	μ_{eff} [μ_B]	x_1 [mol% $Fe_2^{3+}O_3$]	x_2 [mol% $Fe_2^{2+}O_3$]	x_1/x
1	8.3	5.78	0.8	0.2	0.8
3	24	5.67	2.2	0.8	0.73
5	38	5.53	3	2	0.63
10	72	5.38	4.5	5.5	0.45
20	138	5.26	6.6	13.4	0.33

4. Conclusions

Homogeneous glasses were obtained when dissolving Fe_2O_3 in the $3B_2O_3 \cdot KCl$ matrix up to a concentration of 20 mol fraction Fe_2O_3.

Magnetic susceptibility measurements performed on $xFe_2O_3 \cdot (100-x)[3B_2O_3 \cdot KCl]$ glasses with $0<x\leq20$ mol % lead to data depending on the Fe_2O_3 content. These data indicate that in the glasses with x>5 mol % the iron ions participate to negative magnetic superexchange interactions. The Curie constant values allow establishing that in all the glasses both Fe^{3+} and Fe^{2+} ions are present, last being higher for x>5 mol %.

REFERENCES

1. I. Ardelean, M. Peteanu, V. Simon, S. Filip, F. Ciorcas and I. Todor, J. Magn. Magn. Mat. 196/197, 257 (1999).
2. I. Ardelean, P. Pascuta and V. Ioncu, Mod. Phys. Lett. B, 15, 30 (2001).
3. H. H. Wickman, M. P. Klein and D. A. Shirlei, J. Chem. Phys., 42, 2113 (1965).

4. I. Ardelean, Studii si Cercet. de Fizaca, 33, 55 (1981).
5. B. Kumar, C. H. Chen and S. Liu, Phys. Chem. Glasses, 33, 45. (1992).
6. I. Ardelean, M. Peteanu, S. Filip, V. Simon and G. Győrffy, Solid State Commun. 102,341 (1997).
7. L. K. Wilson, E. J. Friebele and D. L. Kinser, Proc. Int. Symp. On Amorphous Magnetism, Plenum Press, New York, 1975, p. 65.
8. E. Burzo and I. Ardelean, Phys. Chem. Glasses, 20, 15 (1979).
9. I. Ardelean, Gh. Ilonca, O. Cozar and G. Muresan, Studia Univ. Babes-Bolyai, Physica, 2, 37 (1989).
10. B. Kumar and C. H. Chen, J. Appl. Phys. 75,6760 (1994).
11. I. Ardelean, Hong-Hua Qiu and H. Sakata, Mater. Lett. 32,335 (1997).
12. I. Ardelean, H. Satou, H. Sakata, Studia Univ. Babes-Bolyai, Physica, XLIII (2), 3 (1998).
13. I. Ardelean, Gh. Ilonca, O. Cozar, V. Simon and S. Filip, Mater. Lett. 21,321 (1994).
14. C. M. Hurd, Contemp. Phys. 23, 469 (1982).
15. B. J. Friebele, L. K. Wilson, A. W. Dozier and D. L. Kinser, Phys. Status Sol (b), 45,323 (1971).
16. L. M. Mulay, Magnetic Susceptibility (Interscience, New York, 1973) p. 1773.

STUDIA UNIVERSITATIS BABEŞ-BOLYAI, PHYSICA, XLVII, 2, 2002

MAGNETIC SUSCEPTIBILITY INVESTIGATION OF SAMARIUM IONS IN $2B_2O_3 \cdot Li_2O$ GLASS MATRIX

I. ARDELEAN

Faculty of Physics, Babes-Bolyai University, 3400 Cluj-Napoca, Romania

ABSTRACT. Magnetic susceptibility measurements have been performed on $xSm_2O_3 \cdot (100-x)[2B_2O_3 \cdot Li_2O]$ glass with $0 < x \leq 40$ mol %. From effective magnetic moment values $\mu_{eff} = (1.60 \pm 0.05)\ \mu_B$ we have established that in these glasses are present only Sm^{3+} ions, which for $x > 10$ mol % participate to the superexchange magnetic interactions.

Introduction

The study of the magnetic properties of oxide glasses with transition element ions is an interesting subject of research. Their analysis give useful information on the valence states and magnetic interactions between these ions in a vitreous oxide matrix, as well as on their distribution in glasses.

Glass formation in the R_2O_3-B_2O_3 systems, where R = Nd or Sm, was studied by Chakraborty et al. [1]. Glasses may be formed in the composition range from 0 to 28 % mol rare-earth oxide. In case of the $xRO \cdot (100-x)[2B_2O_3 \cdot PbO]$ systems where $RO \Rightarrow Gd_2O_3$ [2], Ho_2O_3 [3], Eu_2O_3 [4] and CeO_2 [5] are formed glasses for $x \leq 30$, ≤ 30, ≤ 20 and ≤ 30 mol %, respectively, but in case of the $xPr_6O_{11} \cdot (100-x)[2B_2O_3 \cdot CdO]$ system [6] they are formed for $x \leq 50$ mol %.

The magnetic properties of $xRO \cdot (100-x)[2B_2O_3 \cdot PbO]$ ($RO = Gd_2O_3$ [2], Ho_2O_3 [3], Eu_2O_3 [4] or CeO_2 [5]) and of $xPr_6O_{11} \cdot (100-x)[2B_2O_3 \cdot CdO]$ [6] glasses have previously been reported. Specific magnetic behaviour for these ions in lead- and cadmium-borate oxide glasses was evidenced. The europium, cerium and praseodymium ions, in these glasses are Eu^{2+}, Eu^{3+}, Ce^{3+}, Ce^{4+} and Pr^{3+}, Pr^{4+} valence states, respectively.

As a part of these investigation of oxide glasses with rare-earth ions, we report in this paper the magnetic behaviour of the $xSm_2O_3 \cdot (100-x)$ $[2B_2O_3 \cdot Li_2O]$ glasses.

Experimental

The samples were prepared by mixing H_3BO_3, Li_2CO_3 and Sm_2O_3 of reagent grade purity in suitable proportion over the $0 < x \leq 50$ mol %. The mechanically homogenized mixtures were melted in sintered corundum

crucibles at 1250°C, in an electrical furnace. After being equilibrated at the melting temperature for 0.5 h, the molten material was quenched at room temperarture by pouring onto a stainless-steel plate. The resulted samples were analyzed by means of X-ray diffraction and did not show any crystalline phase up to 40 mol %.

Magnetic susceptibility measurements were performed with a Faraday-type balance in the temperature range 80-300 K.

Results and discussion

The thermal variations of the reciprocal magnetic susceptibilities, for some $xSm_2O_3 \cdot (100\text{-}x)[2B_2O_3 \cdot Li_2O]$ glasses are plotted in Figure 1. These data indicate a Curie-type behaviour for samples with $x \leq 10$ mol % and a Curie-Weiss type one, with negative paramagnetic Curie temperature, θ_p, for glasses with a higher Sm_2O_3 content.

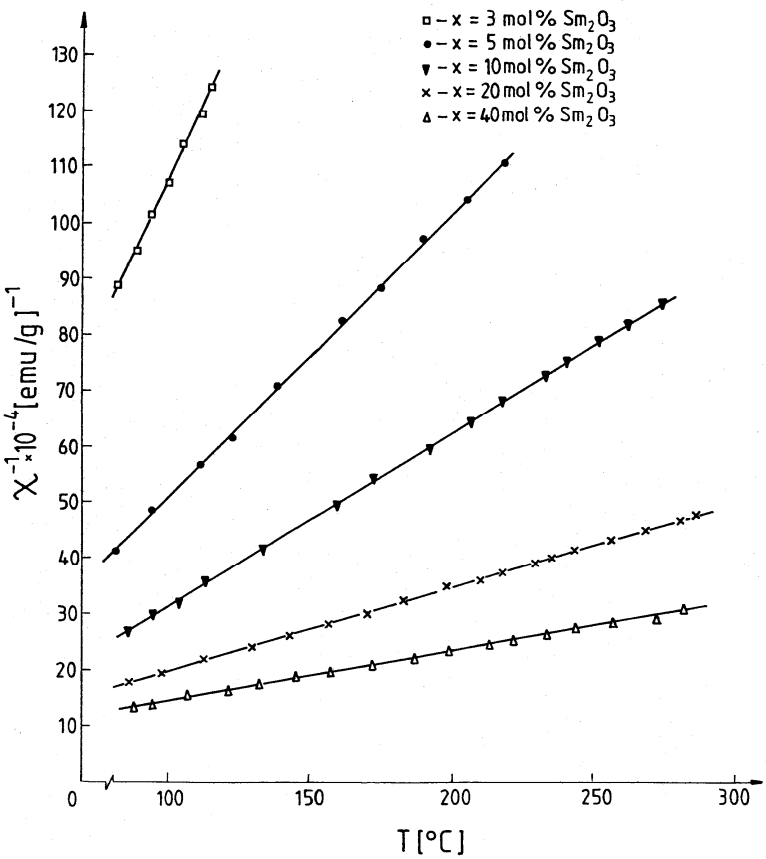

Fig. 1. Temperature dependence of the reciprocal magnetic susceptibility.

These data suggest that the samarium ions are isolated or participate to the dipole-dipole interactions for $x \leq 10$ mol % and antiferromagnetically coupled for higher concentrations, the θ_p increasing in absolute magnitude with these ions concentration (Fig. 2). This reflects an increase of the exchange interactions between samarium ions in studied glasses [7]. This non-linearly increase of θ_p can be datored structural modification of network of glasses studied or different valence states of samarium ions present in these glasses. In the glasses, only short-range magnetic order takes place and this behaviour can be described by a mictomagnetic type order [8].

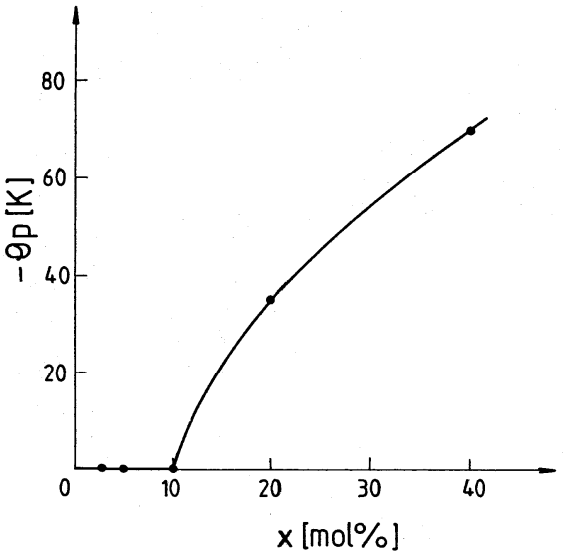

Fig. 2. Composition dependence of the paramagnetic Curie temperature.

In this way the samarium ions have similar behaviour as gadolinium [2], holmium [3], in lead-borate and praseodymium [6] in cadmium-borate oxide glasses, evidencing for $x > 2$ mol %, $x > 0$ mol % and respectively $x > 1$ mol % a Curie-Weiss behaviour, but it differs from that of europium [4] and cerium [5] ions in lead-borate oxide glasses. These data suggest that the nature of rare earth ions and of the glass matrix plays an important role in the distribution mode of rare-earth ions in oxide glass network.

The concentration dependence of the molar Curie constant values, C_M, are given in Figure 3. The experimentally values obtained for C_M and effective magnetic moments, $\mu_{eff} = (1.60 \pm 0.05)\ \mu_B$ (Table 1) are very close to the atomic magnetic moment of Sm^{3+} ion in free ion state $\mu_{Sm^{3+}} = 1.55\ \mu_B$.

The experimentally values obtained for μ_{eff} of Sm^{3+} ions in different paramagnetic salts lie between (1.4 – 1.7) μ_B [9]. The data indicate that in these samples the samarium ions are in Sm^{3+} valence states which determine their specific magnetic behaviour, depending on the Sm_2O_3 content in glasses studied.

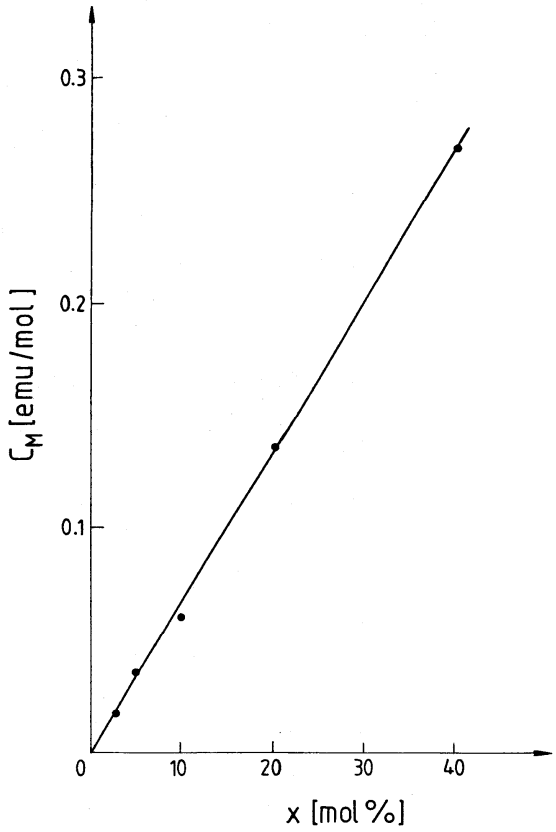

Fig. 3. Composition dependence of the molar Curie constant.

Table 1.

Composition dependence of the molar Curie constants and effective magnetic moments.

x [mol %]	C_M [emu/mol]	μ_{eff} [μ_B]
3	0.01790	1.55
5	0.03456	1.65
10	0.05996	1,56
20	0.1365	1.65
40	0.2648	1.63

Conclusions

Glases of the system $xSm_2O_3 \cdot (100-x)[2B_2O_3 \cdot Li_2O]$ were obtained ower the $0 < x \leq 40$ mol % concentration range.

Magnetic data revealed superexchange – type interactions involving Sm^{3+} ions for $x > 10$ mol %.

REFERENCES

1. I.N.Chakraborty, D.E.Day, J.C.Lapp and J.E.Shelby, J. Amer. Ceram. Soc., 68, 368 (1985)
2. I.Ardelean, E.Burzo, D.Mîtulescu-Ungur and S.Simon, J. Non-Cryst. Solids, 146, 256 (1992)
3. E.Burzo and I.Ardelean, J. Mat. Sci. Lett.,12, 1475 (1993)
4. E.Burzo, I.Ardelean and I.Ursu, Mat. Lett., 26, 10, 3 (1996)
5. E.Burzo, I.Ardelean and D.Mîtulescu, J. Mat. Sci. Lett., 11, 1496 (1992)
6. I.Ardelean, Mod. Phys. Lett. B, 8, 285 (2002)
7. B.J.Friebele, L.K.Wilson, A.W.Dozier and D.L.Kinser, Phys. Status Solidi B, 45, 323 (1971)
8. C.M.Hurd, Contemp. Phys., 23, 469 (1982)
9. E.Burzo, Fizica fenomenelor magnetice, vol. 1, Ed. Acad. Bucuresti, 1979, p.24.

STUDIA UNIVERSITATIS BABEŞ-BOLYAI, PHYSICA, XLVII, 2, 2002

DIELECTRIC PROPERTIES CHANGES INDUCED BY IRON ADDITION TO SiO_2-CaO-P_2O_5 GLASS SYSTEM

V. SIMON, S. FILIP*, I. ARDELEAN, I. BARBUR

Faculty of Physics, Babes-Bolyai University, 3400 Cluj-Napoca
**Physics Department, University of Oradea, 2700 Oradea*

ABSTRACT. Glasses of various compositions in the system $xFe_2O_3 \cdot (22-x)$ $SiO_2 \cdot 60CaO \cdot 18P_2O_5$ were prepared via melt quenching technique. The dielectric properties of samples, dielectric constant ε_r and loss tan δ, were investigated as function of composition ($0 \leq x \leq 12$ mol %), temperature (from room temperature up to 200^{o}C) and frequency (1, 10 and 100 kHz).

Introduction

The properties of glass systems depend upon their composition and to a considerable extend upon their structure. The study of dielectric properties of the glass materials help in assessing their insulating character and may also help in understanding their structure to some extent. Work along these lines was carried out in recent years on a variety of inorganic glasses yielding valuable information [1-5].

Phosphate glasses have several advantages over conventional silicate and borate glasses due to their physical properties such as high thermal expansion coefficient, low melting temperature and high ultraviolet transmission [6-10]. However the poor chemical durability of phosphate glasses prevented them from replacing the conventional glasses in a wide range of technological applications. In the last years there has been lot of studies on improving the physical properties and chemical durability of phosphate glasses by introducing glass formers and modifiers into P_2O_5 glass network [11-15].

Among various phosphate glass systems the calcium phosphate glasses are considered to be relatively stable. The addition to CaO-P_2O_5 glass matrices of SiO_2 may enhance their stability and the addition of Fe_2O_3 may improve their aqueous durability. The objective of this investigation is to follow the changes of dielectric properties of a CaO-P_2O_5-SiO_2 glass matrix caused by addition of different Fe_2O_3 contents.

Experimental

Bulk glassy samples belonging to $xFe_2O_3 \cdot (22-x)SiO_2 \cdot 60CaO \cdot 18P_2O_5$ system were prepared by conventional melt quenching technique from $CaCO_3$, $CaHPO_4 \cdot 2H_2O$, SiO_2 and Fe_2O_3 of reagent grade purity. The mixtures corresponding to the desired compositions ($0 \leq x \leq 12$ mol %) were melted at 1550^{o}C for 10 minutes in an electric furnace Carbolite type RHF 1600, in air, under normal conditions. The melting parameters of the glass samples were chosen in agreement with the phase diagrams of the studied systems [16-18]. The melts were quickly undercooled by pouring onto stainless steel plates at room temperature. Finally the samples were heat treated at 1000^{o}C for 30 minutes and cooled to room temperature in the disconnected furnace.

Capacitance and dielectric loss (tan δ) measurements were carried out using a Keithley 3330 LCZ Meter, from room temperature up to 200^{o}C in the frequency range 1 – 100 kHz on samples polished as plates with plan parallel faces. The dielectric constant was calculated based on the measured capacitance, electrode and sample areas and sample thickness.

Results and discussion

The temperature dependences of the dielectric constant ε_r at different frequencies, for the investigated samples, are depicted in Figure 1. The dielectric loss tan δ of the samples are illustrated in Figure 2.

The dielectric constant ε_r and loss tan δ for the sample without iron ($x = 0$) change insignificantly in the temperature and frequency ranges explored, at least as compared with the iron containing glasses. ε_r is close to 40 and tan $\delta \approx 10^{-2}$. In fact one observes a weak increase also in this case, as is illustrated for ε_r function on temperature in Figure 3.

Relative to the silica-calcium-phosphate matrix the values of dielectric constant are found to decrease and those of loss to increase with introduction of Fe_2O_3 in the first part of the temperature range, depending on frequency. The temperature range, where the dielectric constant of glass matrix is higher than for iron containing samples, narrows when the frequency decreases.

On the other hand, in the entire temperature range and at all investigated frequencies, an increase of ε_r with iron oxide content is noticed in iron containing samples. The results for dielectric loss indicate an increase with Fe_2O_3 addition. The values of tan δ for the sample $x = 4$ and $x = 8$ are very close up to 375 K but above this temperature they are higher for $x = 4$ than for $x = 8$.

The temperature dependences of ε_r at 1, 10 and 100 kHz indicate a slow increase for the samples containing up to 8 mol % Fe_2O_3 while the dependence for the sample containing 12 mol % Fe_2O_3 is more pronounced. On the other hand, in the last case, the dependence is no more linear, as

can be observed from Figure 1. The value of ε_r at 475 K and 1 kHz is around 250 and at the same temperature is diminished about 1.8 times as the frequency increases with an order of magnitude, while at 300 K the measurements indicate $\varepsilon_r \approx 25$ at 1 kHz, an decrease to $\varepsilon_r \approx 20$ at 10 kHz and to $\varepsilon_r \approx 15$ at 100 kHz, i.e. about 1.3 times as the frequency increases with an order of magnitude. The results are in agreement with the data reported for other glasses and glass-ceramics containing transition metal oxides [19,20]. The relative high dielectric constant of SiO_2-CaO-P_2O_5-Fe_2O_3 system at room temperature, particularly at low frequency, may be ascribed to the bonding defects produced in the sample network which contribute to the space charge polarisation [20, 21].

With respect to the dielectric loss the results are apparently similar with the remark that the values measured for the samples containing 4 and 8 mol % Fe_2O_3 are very close in the first part of the temperature range, up to 375 K, and further their evolution is reverted with respect to the temperature dependence recorded for dielectric constants at all frequencies. The dielectric loss in iron containing samples is mainly attributed to the iron ions conduction, that could explain the increase of tan δ with Fe_2O_3 content

The dielectric behaviour is determined by contributions from electronic, ionic, dipolar and space charge polarisations. Among these the space charge polarisation depends on the purity and perfection of the glasses. The changes in dielectric properties of the investigated glass samples could be also understood considering the changes occurred in the structural units and arrangements in the glass network [22].

Silica-calcium-phosphate glasses containing iron have a complex composition and are an admixture of network formers and modifiers. Both SiO_2 and P_2O_5 are glass formers. Pure vitreous SiO_2 and P_2O_5 consist in a continuos random network of quasi-tetrahedral SiO_4 and PO_4 units wherein silicon, respectively phosphorous is four coordinated. The structure of phosphate glasses can be correlated with Q^n terminology, first introduced for silicate glasses and also adopted for phosphate ones [23], where n is the number of bridging oxygens in a tetragonal unit. In this case Q^o represents isolated tetrahedra. The presence of the modifier like alkali and alkaline earth species decreases the number of bridging oxygens (Si-O-Si or P-O-P bridge) in SiO_4 or PO_4 units. The tetrahedrons are linked together in chains or rings by bridging oxygens. The neighbouring chains are linked together by non-bridging oxygens.

CaO and Fe_2O_3 act as glass network modifiers. CaO is a well known glass modifier and may enter the glass network by transforming two Q^3 tetrahedra into two Q^2 tetrahedra and thus a CaO polyhedron is formed when it is surrounded by such two Q^2 and several Q^3 tetrahedrons [20]. This structure behaves as a defect in the network of tetrahedral units [24].

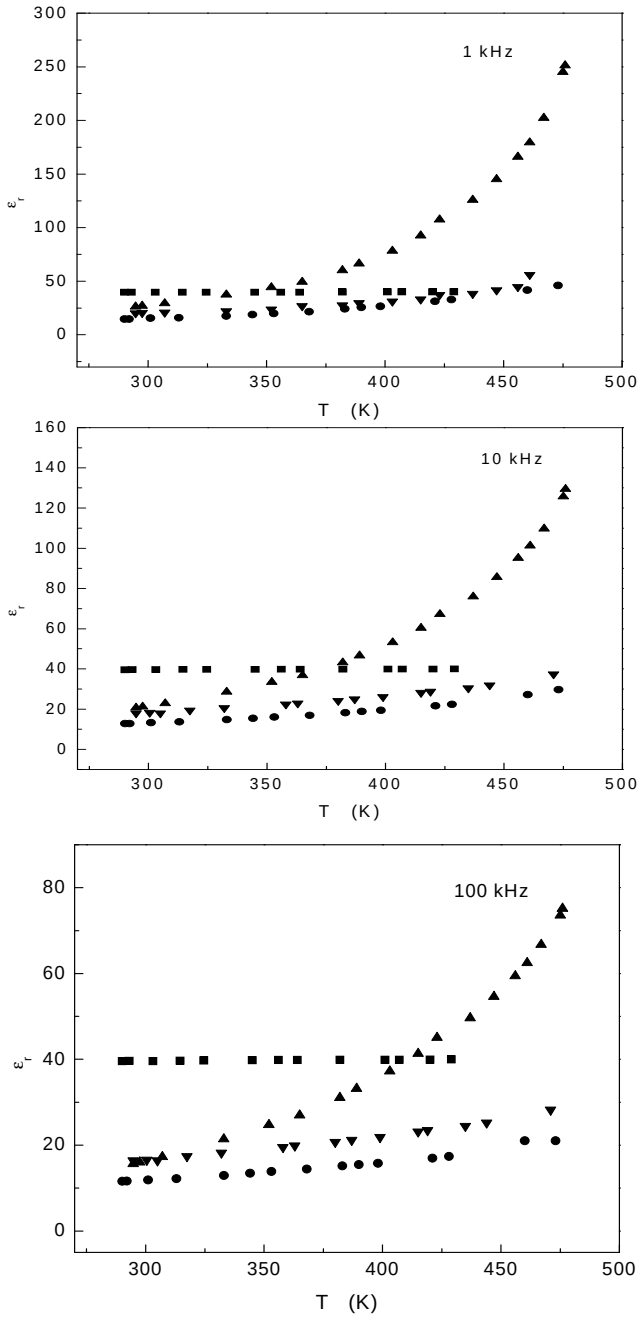

Fig.1. Temperature dependece of dielectric constant at different frequencies for x = 0 (▪), x = 4 (●), x = 8 (▼) and x = 12 (▲).

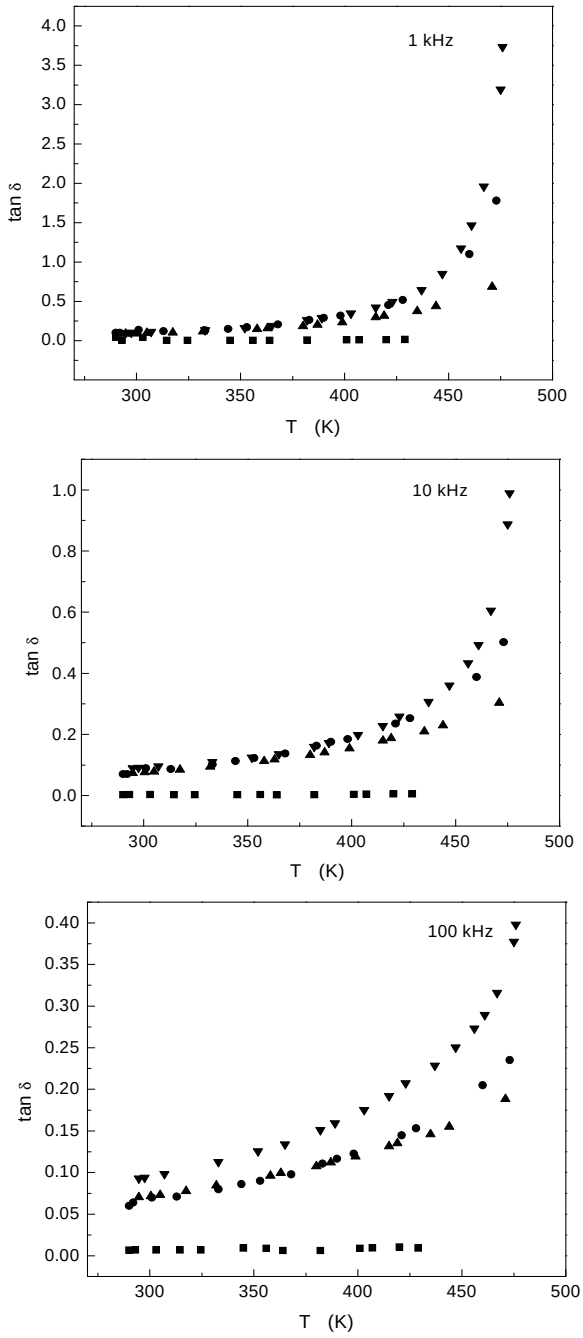

Fig. 2. Temperature dependece of dielectric constant at different frequencies for x = 0 (▪), x = 4 (●), x = 8 (▼) and x = 12 (▲).

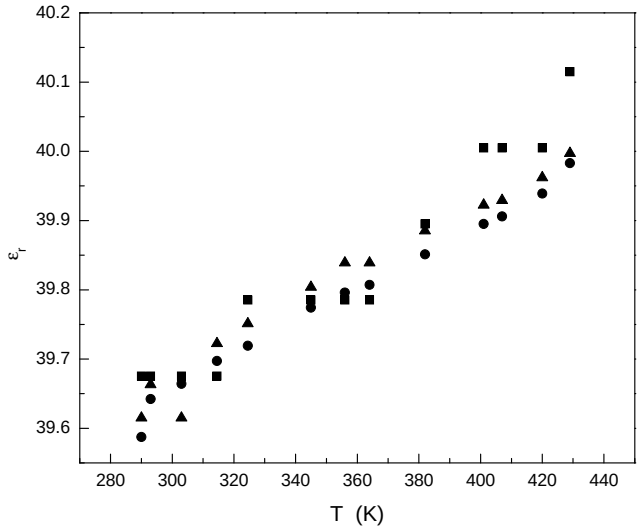

Fig. 3. Dielectric constant of the sample without iron versus temperature at frequencies of 1 kHz (▪), 10 kHz (●) and 100 kHz (▼).

Generally, the increase of glass temperature determines weak changes in the electronic and ionic polarisations. The data obtained for the samples with $0 \leq x \leq 8$ mol % Fe_2O_3 verify these considerations but those for x = 12 mol % point out a large variation of ε_r and tan δ with temperature. Such a behavior can be assigned to space charge polarisation changes due to the bonding defects [20].

Therefore the progressive addition of iron concentration in the P_2O_5-CaO-SiO_2 matrix increases the degree of deformation of glass network with increasing bonding defects, which in turn increases the space charge polarisation causing an increase in the values of dielectric parameters.

Conclusions

In the iron containing lime-silica-phosphate glasses the dielectric constants and the dielectric loss are found to decrease with increase in frequency for all the compositions under study. The dispersion is higher at lower frequencies.

The samples are characterised by relative high dielectric constant, denoting bonding defects in the glass network. At all temperature and frequencies investigated the dielectric loss for P_2O_5-CaO-SiO_2 matrix is lower than for iron containing samples. The dielectric constant is higher for the glass matrix than for iron containing samples only in the first part of the temperature range, depending on frequency.The dielectric loss in iron containing samples is mainly attributed to the iron ions conduction.

These changes in the dielectric parameters with the composition, temperature and frequency indicate that the progressive addition of iron to the glass matrix gradually increases the deformation degree of glass network.

REFERENCES

1. M.D. Ingram, Phys. Chem. Glasses, 28, 215 (1987)
2. A.A. Bahgat, M.M. Samanoudy, A.I. Sabry, Phys. Chem. solids, 60, 1921 (1999)
3. R. mallawani, Mater. Chem. Phys., 37, 224 (1994)
4. V.R. Kumar, N. Veeraiah, Phys. Status solisi A, 147, 601 (1995)
5. G.S. Rao, N. Veeraiah, Eur. Phys. J. Appl. Phys., 19, 11 (2001)
6. B.J. Ainslie, S.P. Craig, S.T. Davey, A.S.L. Gomes, Mater. Sci. Lett., 6, 1361 (1987)
7. K.B. Richard, J. Non-Cryst. Solids, 263-264, 1, (2000)
8. S.W. Lee, J.H. Lee, J. Phys. Chem. Glasses, 36, 127 (1995)
9. Y.B. Peng, D.E. Day, Glass Technol., 32, 166 (1991)
10. W. Matz, D. Stachel, E.A. Goremychkin, J. Non-Cryst. Solids, 101, 80 (1988)
11. A. Mogus-Milankovic, D.E. Day, J. Non-Cryst. Solids, 263-264, 299, (2000)
12. L. Montagne, G. Palavit, Phys. Chem. Glasses, 38, 15 (1997)
13. K. Muruganandam, M. seshasayee, Phys. Chem. Glasses, 40, 287 (1999)
14. B.V.R. Chowdari, A.K. Akhter, Solid State Ionic, 28, 747 (1988)
15. C.T. Chia, B.V.R. Chowdari, K.L. Tan, J. Mater. Sci., 28, 35,94 (1993)
16. K. Koch W. Fix, Arch. Eisentuettenwes., 41, 2, 111 (1970)
17. B. Phillips, A. Muan, J. Am. Ceram. Soc., 41, 11, 445 (1958)
18. J.H. Welch, W.H. Gutt, J. Am. Ceram. Soc., 42, 1, 11 (1959)
19. G.S. Murugan, K.B.R. Varma, J. Non-Cryst. Solids, 279, 1 (2001)
20. P. Subbalkshmi, N. Veeraiah, J. Non-Cryst. Solids, 298, 89 (2002)
21. V.R. Kumar, N. Veeraiah, J. Phys. Chem. Solids, 59, 91 (1998)
22. A. Rulmont, R. Cahay, P. Tarte, Eur. J. Solid State Inorg. Chem., 28, 207 (1991)
23. R.K.Brow, T.M.Alan, D.R.Tallant, RR.J.Kirkpatrick, MRS Bull., 23, 11, 63 (1998)
24. K. Meyer, Phys. Chem. Glasses, 39, 108 (1998)

STUDIA UNIVERSITATIS BABEŞ-BOLYAI, PHYSICA, XLVII, 2, 2002

NMR OBSERVATION OF THE SPIN-SPIN RELAXATION IN POLYBUTADIENE-C_6H_{12} AND POLYBUTADIENE-C_6D_{12} SOLUTIONS

M. TODICA

"Babes-Bolyai" University, Faculty of Physics, 3400 Cluj-Napoca.

ABSTRACT. The comparative analyze of the relaxation curves of the transversal magnetization of the protons of polybutadiene-C_6H_{12} and polybutadiene-C_6D_{12} solutions is done in order to established the contribution of the polymer and the solvent to the spin-spin relaxation process.

Introduction

The mobility of the polymeric segments above the glass transition temperature, is strongly influenced by the presence of solvent molecules in the vicinity of the polymeric chain, [1,2]. Generally this mobility increase with increasing temperature and solvent concentration and induces important modifications of the magnetic interaction between the nuclear spins attached to the polymeric chain. The magnetic behavior of these spins can be investigated by NMR method, observing the relaxation of the transversal magnetization, [3]. The NMR method can be applied to every kind of nucleus heaving non zero magnetic momentum, but the proton are one of the most observed nuclear spin. The hydrogen is one of the most important component of every polymer or solvent and the resonance of the protons is easy to observe because its great gyromagnetic factor γ. But the majority of the solvents used in polymeric solutions contains protons, so that the total transversal magnetization observed by NMR method in the polymeric solutions is determined both by the protons of the polymer and of the solvent. It is important in this case to analyze the contribution of each component of the solution, the polymer and the solvent to the total transversal magnetization. For this aim a comparative study of polymeric solutions containing protonated and deuterated solvent are of the great utility.

In this work we observed the relaxation of the transversal magnetization of the protons in some polybutadiene-C_6H_{12} and polybutadiene-C_6D_{12} solutions in order to established the contribution of the solvent and polymer protons to the relaxation processes.

Experimental

We studded the polybutadiene PB 1009 with the molecular mass M_n=70000[g/moll] and the microstructure 8% vinyl, 38% "cis" and 54% "trans". The glass transition temperature of this polymer is T_g=175K. The solvent was

the protonated cyclohexane C_6H_{12} and the deuterated cyclohexane C_6D_{12}. We studded two solutions with the same concentration of the polymer 80%, the polybutadiene-C_6H_{12} , (PBH) and the polybutadiene-C_6D_{12} , PBD). The samples were enclosed in NMR tubes and sealed under primary vacuum. The relaxation of the transversal magnetization was measured using the standard Carr-Purcell sequence, [4]. All the measurements were performed using a Bruker CXP spectrometer working at 36MHz, in the temperature range 250-330K.

Results and discussion

The relaxation of the transversal magnetization of the protons was observed for the protonated and deuterated polymeric solutions at the same concentration and temperature, (Fig.1).

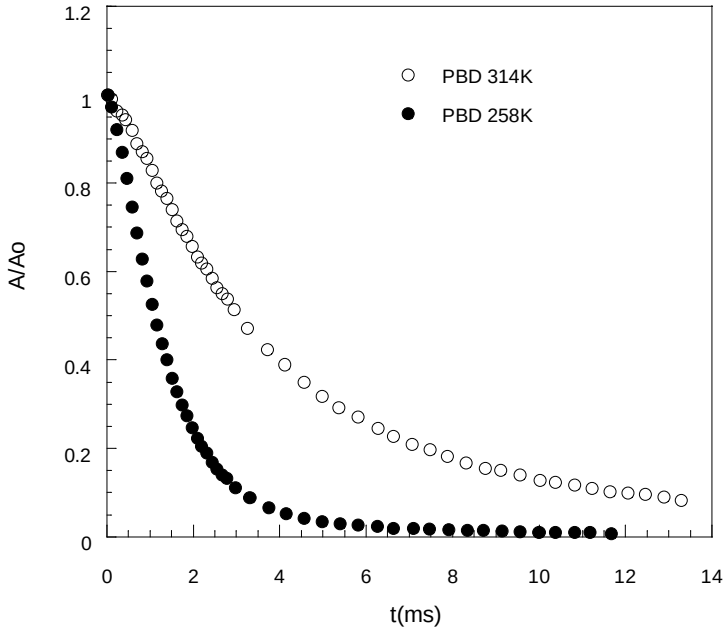

Fig.1. Relaxation curves of the polybutadiene-C_6D_{12} solution at T=258K and T=314K

The protonated and deuterated cyclohexane molecules have the same structure and dynamic properties and present the same interaction with the polymer, so that, the two kind of polymeric solutions are equivalent of the point of view of the dynamics. For this reason, we can consider that the dynamic behavior of the polymeric chain, for a given concentration of the solvent, is the same in both solutions. The difference is that the transversal magnetization is determined only by the protons of the polymer, in the case of C_6D_{12} solvent and both by the protons of the polymer and of the solvent, in the case of C_6H_{12} solvent.

The analyze of the relaxation curves of the solution containing deuterated solvent, give information only about the relaxation of the transversal magnetization of the polymer. We can distinguish two parts of these curves; the fast decay of the magnetization, in the range of few milliseconds, at the beginning of the relaxation processes and the slow decay of the magnetization, in the range of ten milliseconds, at the end of the relaxation. This behavior is characteristic for the polymeric materials and it is associated with different dynamic parts of the polymeric chain, [5,6]. The fast decay is associated with the rigid part of the chain, (the polymeric segment including one or more monomers) and the slow decay is associated with the parts of the chain heaving great mobility, like the ends of the chain. For this reason the experimental data can't be described by a single exponential function and the relaxation processes can't be characterized by a single relaxation time T_2.

We can observe also that the shape of the relaxation curves are function of temperature. At low temperature, for example at T=258K, the relaxation is very fast, the amplitude of the transversal magnetization falls near zero in very short time, about 4ms and the amplitude corresponding to the terminal relaxation is practically zero. We can assume that the relaxation processes is mainly determined by the rigid part of the polymeric chain. When the temperature increases, at T=314K for example, the range time corresponding to the fast relaxation is greater, about 4ms, and the terminal relaxation is extended over many tens milliseconds. The delimitation between the two regions is not so sharp like at low temperatures, but also in this case we can observe the two domains of the relaxation. This behavior indicates an increasing of the mobility of the entire chain, [7,8].

The analyze of the experimental data corresponding to the polybutadiene-C_6H_{12} solution shows also the existence of two parts of the relaxation curves, like in the case of the polybutadiene-C_6D_{12} solution, (Fig. 2.) We can observe that the shape of the relaxation curves in the fast region is practically the same for both the solutions containing protonated and deuterated solvents. That means that the decay of the transversal magnetization in both the cases is very similar. But for polybutadiene-C_6H_{12} solution the transversal magnetization is determined both by the protons of the solvent and the protons of the polymer, which has different rates of relaxation. The similarity between the relaxation curves in the fast domain of the polybutadiene-C_6H_{12} and polybutadiene-C_6D_{12} solutions, can be explained only if we assume that the relaxation of the solvent protons is a very slow processes, extended on the range of hundreds milliseconds or few seconds. The contribution of these protons to the fast decay of the relaxation curves could be regarded as a constant. This constant do not modifies the slope of the relaxation curve in the fast domain. Indeed the transversal magnetization of the polymer falls to zero after few milliseconds. If the total magnetization should be determined

only by the protons of the polymer, then the relaxation curve should decreases to zero in this time interval. But we can see from figure 2 that in the case of sample polybutadiene-C_6H_{12} the transversal magnetization do not completely falls in this time domain. This fact indicates that in addition to the polymer, there are another contribution to the total magnetization, which can be regarded as a constant in this time domain. This contribution is determined by the rotons of the solvent.

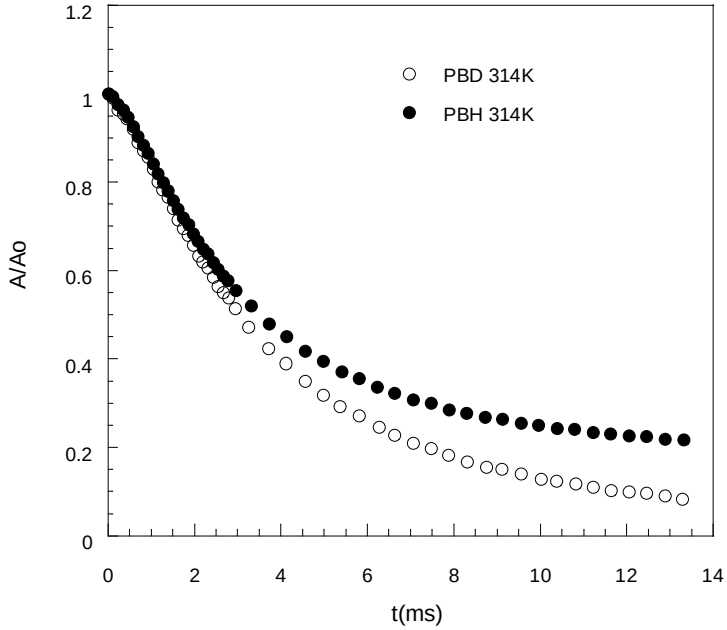

Fig.2. Relaxation curves of the polybutadiene-C_6D_{12} and polybutadiene-C_6H_{12} solution at 314K

Difference between the curves describing the relaxation of two samples, polybutadiene-C_6H_{12} and polybutadiene-C_6D_{12} solutions, appears in the region of the terminal relaxation of the polymer. For the polybutadiene-C_6H_{12} solution, the amplitude of the transversal magnetization do not fall completely like in the case of the deuterated sample, (Fig.2). That means that the relaxation processes in this temporary range, is mainly determined by the protons of the solvent. We can also observe that the decay of the relaxation curves in this region is very slow, which is in accord with the supposition that the relaxation rate of the solvent is much smaller than that of the polymer.

That comparative analyze of the experimental data shows that the relaxation of the transversal magnetization of the protons of the polybutadiene and cyclohexane are very different. The relaxation of the polymer is a fast

processes giving contribution at the beginning of the relaxation curves and the relaxation of the protons of the cyclohexane is a slow processes with major contribution on the terminal region. Taking into account the similitude of relaxation curves in the fast domain, we can conclude that preliminary information concerning the relaxation process of the polymer can be obtained by analyzing the relaxation curves of the polybutadiene-C_6H_{12} or polybutadiene-C_6D_{12} solutions in this domain of relaxation.

Conclusion

The comparative analyze of the relaxation curves of the transversal magnetization of the protons, recorded from the polybutadiene-C_6H_{12} and polybutadiene-C_6D_{12} solutions with the same concentration and to the same temperature, allows to establish the contribution of the polymer protons and solvent protons to the entire relaxation processes.

The relaxation curves recorded for both kind of samples are characterized by two parts, the fast decay and slow decay.

The fast relaxation processes is determined mainly by the protons of the polymer and the slow processes is governed by the protons of the solvent.

REFERENCES

1. J. D. Ferry, Viscoelastic Properties of Polymers, Wiley, New York, 1983.
2. P. G. De Gennes, Scaling Concepts in Polymer Physics, Cornell University Press, Ithaca, 1979.
3. J. P. Cohen-Addad, Physical Properties of Polymeric Gels, John Wiley and Sons, Chicester, 1996.
4. H.Y.Carr and E.M. Purcell, Phys. Rev., 1954, 94, 630.
5. J. P. Cohen-Addad, NMR and Fractal properties of Polymeric Liquids and Gels, Pergamon Press, London, 1992.
6. J. P. Cohen-Addad, A. Labouriau, J. Chem. Phys., 93, (4), 1990, 2911-2918
7. A. Labouriau, J. P. Cohen-Addad, J. Chem. Phys., 94, (4), 1991, 3242-3250.
8. M. Todica, These, Univ. Joseph. Fourier, Grenoble, 1994.

STUDIA UNIVERSITATIS BABEŞ-BOLYAI, PHYSICA, XLVII, 2, 2002

ANALYSIS OF THE ATTENUATION OF THE SPIN-ECHO IN THE PRESENCE OF THE MAGNETIC FIELD GRADIENTS

M. TODICA

"Babes-Bolyai" University, Faculty of Physics, RO-3400 Cluj-Napoca, Romania

ABSTRACT. Different methods for the analyze of the spin-echo attenuation in the NMR pulsed field gradient experiments were used for investigating the diffusion process in pure ethanol and polyoxiethylene gel gonfled with ethanol.

Introduction

Many properties of the polymeric materials, like the viscoelasticity, the mechanical behavior, are determined by the local dynamics of the monomeric units of the polymeric segments, [1,2]. There are many methods to study this dynamics, but NMR is one of the most useful technique because its noninvasive character and the great accuracy of the results. Generally the analyze of the spin-lattice or spin-spin relaxation process of the nuclear spins attached to the polymeric chain, are the most utilized ways in this aim [3,4]. These methods leads to indirect observations of the local mobility of the nuclear spins.

Direct observation of the diffusion process of the nuclear spins is possible by using the magnetic gradient NMR technique. This method is based on the supplementary attenuation of the spin-echo in the presence of the applied magnetic field gradient. There are many variety of NMR sequences utilized in this aim, but all are based either on the use of the constant magnetic field gradient [5], or the use of pulsed magnetic field gradient, [6,7]. In all the cases the spin-echo attenuation is analyzed as a function of the amplitude or the duration of the applied magnetic field gradient. For samples containing a single kind of diffusing spins, the analyze is generally simple. When the sample contains two or more species of diffusing spins, like in the case of polymeric solutions, the use of only one method of analyze can leads to errors in the evaluation of the diffusion coefficient.

In this work we present different methods of analyze of the spin-echo attenuation in order to established the contribution to the diffusion process of one or more kind of diffusing spins. We tested these methods for two samples, the pure ethanol and the polyoxiethilene gel gonfled with ethanol, (POE–ethanol).

Experimental

All the measurements were performed using standard NMR CPX Bruker spectrometer working at 60 Mhz. The diffusion was investigated using the basic Stejskal-Tanner pulse sequence, by varying the amplitude of the magnetic field gradient, [6]. All the time delays of the sequence are kept constants. The gradient is produced with a antihelmholtz coils pair and has the amplitude $g = \alpha \cdot U$, where the constant α has the value α = 0.14 gauss/(cm mV) and U is the electric tension applied to the gradient coils, [11]. The samples were enclosed in NMR tubes with the diameter 4mm and sealed under primary vacuum. The temperature was kept constant, T=298K.

RESULTS AND DISCUSSION

The basic pulse sequence for measuring the diffusion coefficient is based on the Hahn spin-echo sequence $\left(\frac{\pi}{2}\right)_{x'} - \tau - (\pi)_{x'} - \tau - \text{echo}$, performed in the presence of the magnetic field gradient superimposed on the main magnetic field $\vec{B}_0$. The magnetic field gradient $\vec{G}$ is parallel to $\vec{B}_0$ and can be applied continuously during the delay time τ between the two radiofrequency pulses, or it can be applied on the form of two pulses intercalated between the radiofrequency pulses.

The first description of the attenuation of the spin-echo in the presence of the constant magnetic field gradient, was done by Carr [5] and Torrey [7] and the first description of the pulse method was done by Stejskal and Tanner, [6]. Further developments of diffusion methods, were based on these basic sequences.

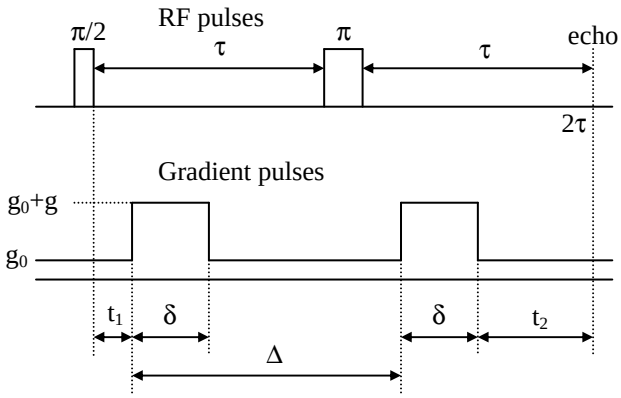

Fig.1. The radiofrequency and gradient pulse sequence.

The explicit expression of the spin-echo attenuation depends on the mode that the gradient is applied. For a constant gradient, the amplitude A(2τ) of the echo is given by the expression, [5]:

$$A(2\tau) = A(0)\exp\left(-\frac{2\tau}{T_2} - \frac{\gamma^2 D \cdot 2\tau^3}{3} \cdot G^2 \right) \quad (1)$$

D is the diffusion coefficient and A(0) is the amplitude of the transversal magnetization at the moment t=0.

For the pulse gradient method, the amplitude of the echo is given by the relation, [8]:

$$A(2\tau) = A(0)\exp\left[-\frac{2\tau}{T_2} - \gamma^2 D\left\{ \delta^2\left(\Delta - \frac{1}{3}\delta \right) g^2 - \delta\left[\left(t_1^2 + t_2^2 \right) + \left(t_1 + t_2 \right)\delta + \frac{2\delta^2}{3} + 2\tau^2 \right] g \cdot g_0 \right\} - 2\gamma^2 D\tau^3 g_0^2 / 3 \right] \quad (2)$$

where the delay times δ, Δ, t_1, t_2 are defined from the figure 1.

G is the total gradient, which include the applied gradient g and the residual gradient g_0. The residual gradient g_0 is determined by the inhomogeneities of the local magnetic field. The equations (1) and (2) can be used in the case of non restrictive diffusion and for a single kind of diffusing spins.

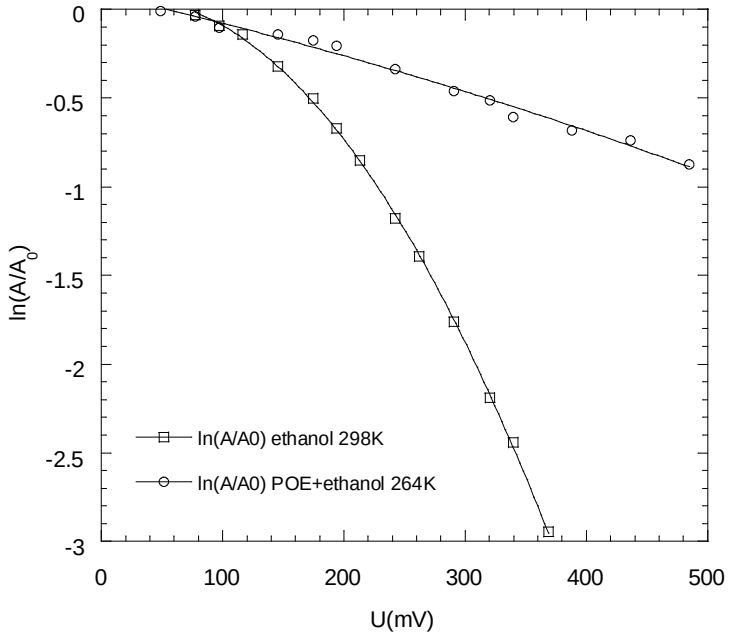

Fig. 2. Polynomial representation of second degree of the attenuation of the spin-echo in function of variable U

We will focused our attention on the pulse gradient method. In the relation (2) the amplitude of the echo can be measured either by varying the amplitude of the applied gradient or varying the length of the time delay of the sequence. Generally the time intervals are kept constant and only the amplitude of the gradient is varied.

For a given pulse sequence, the amplitude of the echo is measured firstly in the absence of any applied gradient, $A(2\tau)_0$ and then for different values of the applied gradient g, $A(2\tau)g$. When the gradient g is zero, from relation (2) we obtain

$$A(2\tau)_0 = A(0)\exp\left(-\frac{2\tau}{T_2} - \gamma^2 D 2\tau^3 g_0^2/3\right) \tag{3}$$

Dividing the relations (2) an (3) we can eliminate the effect of the relaxation and we obtain a new equation, from which we can calculate the diffusion coefficient D.

$$\ln\frac{A(2\tau)_g}{A(2\tau)_0} = \left[-\gamma^2 D\left\{\delta^2\left(\Delta - \frac{1}{3}\delta\right)g^2 - \delta\left[\left(t_1^2 + t_2^2\right) + (t_1 + t_2)\delta + \frac{2\delta^2}{3} + 2\tau^2\right]g \cdot g_0\right\}\right] \tag{4}$$

Equation (4) represents a polynomial function of second degree by rapport of the variable g. The diffusion coefficient can be calculated by many ways.

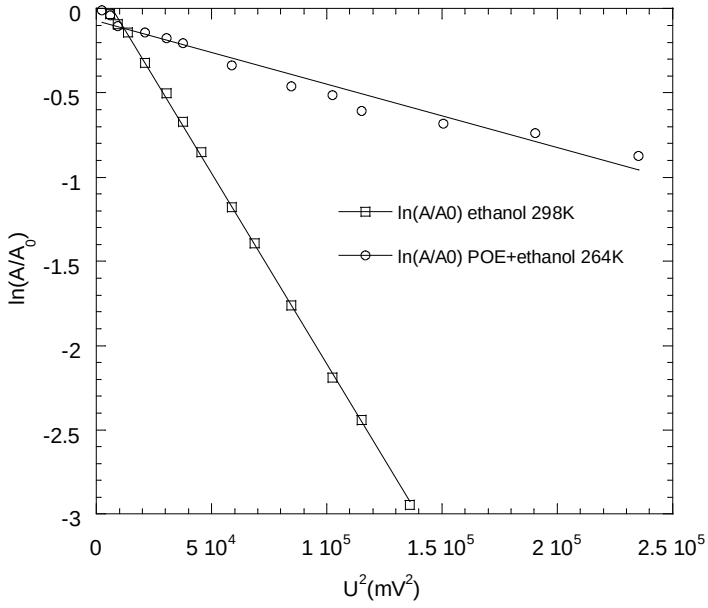

Fig. 3. Representation of the attenuation of the spin-echo in function of variable U^2

a) The experimental data $\ln\left[\frac{A(2\tau)_g}{A(2\tau)_0}\right]$, are represented in function of the variable g and fitted with a polynomial function of second degree, $y=m_0+m_1\cdot g+m_2\cdot g^2$. The value of D results from the coefficient of g^2 of this function, $m_2=-\gamma^2 D\left[\delta^2\left(\Delta-\frac{1}{3}\delta\right)\right]$. This kind of representation is shown in figure 1, for pure ethanol at T=298K and polyoxiethylene gel gonfled with ethanol at 264K. We can observe that in both cases the experimental data $\ln\left[\frac{A(2\tau)_g}{A(2\tau)_0}\right]$ represents curves, which can be approximate with polynomial function.

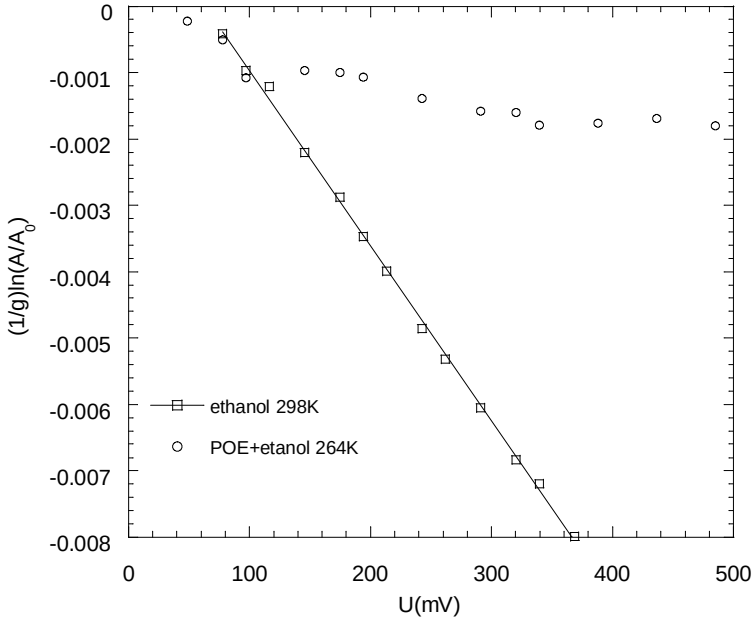

Fig. 4. Representation of the spin-echo attenuation in function of variable U

This kind of representation is not very useful because, for a given set of experimental data, we can find always one polynomial function of second degree passing through these points, but without physical signification. It is the case of POE-ethanol. The experimental data seems to represent a polynomial function of second degree, but in reality the function is more complicated, because this sample contain two kind of diffusing spins, the protons of ethanol and the protons attached to the polymeric chains. It is

clear in this situation that the experimental data do not represent a single polynomial function of second degree.

b) The experimental data $\ln\left[\frac{A(2\tau)_g}{A(2\tau)_0}\right]$, are represented in function of the variable g^2 , equation (4). This situation is shown in figure 3. We obtained linear representations for the pure ethanol and the coefficient D is calculated from the slope of the graphic. In the first approximation we can consider that the representation is linear even in the case of POE-ethanol. However this kind of representation mask the effect of the factor containing the residual gradient g_0 which can induces deviations from the linearity. This representation can be applied only if the residual gradient g_0 can be neglected.

c) The representation $\frac{1}{g}\ln\left[\frac{A(2\tau)_g}{A(2\tau)_0}\right]$ in function of variable g, [9,10].

Equation (4) became:

$$\frac{1}{g}\ln\frac{A(2\tau)_g}{A(2\tau)_0}=\left[-\gamma^2 D\left\{\delta^2\left(\Delta-\frac{1}{3}\delta\right)g-\delta\left[\left(t_1^2+t_2^2\right)+\left(t_1+t_2\right)\delta+\frac{2\delta^2}{3}+2\tau^2\right]g_0\right\}\right] \quad (5)$$

The contribution of the applied gradient g and the residual gradient g_0 to the attenuation of the spin-echo are now clearly separated. The right side of equation (5) became a linear function by rapport to the variable g. If the attenuation of the spin-echo is determined only by a single kind of the diffusing spins, then the experimental data will represent a line. The slope of this line is not affected by g_0. The coefficient D results from the slope:

$$\mathrm{tg}\alpha=-\gamma^2 D\left[\delta^2\left(\Delta-\frac{1}{3}\delta\right)\right] \quad (6)$$

This kind of representation is shown in figure 4. We obtained linear representations for ethanol and a nonlinear representation for POE-ethanol system.

For ethanol there are only a single kind of diffusing spins, and the diffusion process is not limited by other factors. The attenuation of the echo is completely described by equation (2). Every kind of representation: a), b) or c) leads to the same results and the values of D calculated by these methods are very closed each to other, (Table 1.)

The situation is different in the case of POE-ethanol. If we use only the representation a) or b) it seems that the experimental data can be described by equation (4) like in the case that the attenuation of the echo should be determined only by a single kind of diffusing spins. We can calculate an apparent diffusion coefficient D_{app}, but this value will include also the contribution of the solvent and the polymer and will be affected by great errors, (See table 1). It is very difficult to distinguish the two processes.

Representation c) do not leads to a linear function, that clearly indicates that the attenuation of the spin-echo is not determined by a single diffusion process, (figure 3). Indeed, this sample contains two kind of diffusing spins with different mobility, the protons attached to the polymeric chain and the protons of the ethanol. Equation (2) must be completed with supplementary terms including the contribution of both kind of spins to the spin-echo. If we apply the simplest equation (5) we obtain non linear representation, because this equation is valid only for a single kind of diffusing spins. It is clear in these conditions the benefit of using representation c) to establish if the diffusion process is concerned with one or more kind of diffusing spins.

Table 1

Sample/D	Representation a) [cm^2/s]	Representation b) [cm^2/s]	Representation c) [cm^2/s]
Ethanol 298K	$1.04 \cdot 10^{-5} \pm 10\%$	$0.945 \cdot 10^{-5} \pm 10\%$	$1.10 \cdot 10^{-5} \pm 10\%$
POE+Ethanol 264K	$4.038 \cdot 10^{-7} \pm 10\%$	$1.57 \cdot 10^{-6} \pm 10\%$	$3.59 \cdot 10^{-6} \pm 10\%$ $2.06 \cdot 10^{-6} \pm 10\%$

Some remarks can be mentioned in this case. The dynamics of the ethanol is much greater than those of the polymer, so that the main contribution to the attenuation of the spin-echo is determined by the diffusion of the ethanol. If we can neglect the contribution of the polymer to the attenuation of the spin-echo, we can approximate the experimental data by a linear function, (Eq. 5) and we can calculate the coefficient D from the slope of this representation, which will represent the diffusion coefficient of the ethanol of sample POE-ethanol. Taking into account all the experimental data or only the experimental data which describe a line, figure (4), we calculated the extreme values of the diffusion coefficient, (Table 1). It is clear that the value of D will be affected by errors because the contribution of the polymer was neglected. However the order of magnitude of D is the same like in the case of pure ethanol, that indicates that the algorithm c) can be used for preliminary evaluation of the diffusion coefficient even for the sample POE-ethanol.

CONCLUSSION

The diffusion of the nuclear spins can be observed using the NMR magnetic field gradient techniques.

The attenuation of the spin-echo, in the case of the basic pulse magnetic field experiment for diffusion, is described by the Stejskal-Tanner equation. The experimental data can be analyzed in many ways:

-representation by polynomial function of second degree, (algorithm a).
-linear representation in function of variable g^2, (algorithm b).
-linear representation in function of variable g, (algorithm c).

All representation lead to the same results if the attenuation of the spin-echo is determined by a single kind of diffusing spins.

If differences between the results of the three representation appears, that means that the diffusion process is more complicated, including many kind of diffusing spins or restriction diffusion conditions.

The algorithm c) is very useful to establish the existence of many kinds of diffusing spins. This algorithm leads to linear representation if the diffusion is concerned with a single kind of spins and leads to non linear representation if the diffusion is concerned with many kinds of spins.

REFERENCES

1. J. D. Ferry, Viscoelasticity of Polymers, Third ed., Wiley, New York, 1980.
2. P. G. De Gennes, Scaling concepts in polymers physics, Cornell University Press, Ithaca, New-York, (1979).
3. J. P. Cohen-Addad, Physical properties of polymeric gels, J. Wiley, Chicester, (1996).
4. J. P. Cohen-Addad, NMR and fractal properties of polymeric liquids and gels, Pergamon Press, London, (1992).
5. H. Y. Carr, E. R. Purcell, Phys. Rev., 94, 630, (1954).
6. E. O. Stejskal, J. E. Tanner, J. Chem. Phys. 1965, 42, 288.
7. H. C. Torrey, Phys. Rew., 104, 563, (1956).
8. D. M. Grant and R.. K. Harris editors, Encyclopedia of NMR, John Wiley and Sons, Chicester, vol. 3, (1996).
9. M. Todica, Metode aplicative de rezonanta magnetica nucleara, Presa Universitara Clujeana, (2001).
10. R. Casalegno, O. Cozar editors, Methodes avanceess d`analyse spectroscopique . Applications, Presa Universitara Clujeana, (2001).
11. M. Todica, These, Univ. Joseph Fourier, Grenoble, 1994.

STUDIA UNIVERSITATIS BABEŞ-BOLYAI, PHYSICA, XLVII, 2, 2002

TOTAL SOLAR ECLIPSE OF 1999 AUGUST 11

P.M. ABDULRAHMAN, ARAS SAIED MAHMOOD, S.M. MAMAND

Department of Physics/College of Science/University of Sulaimani
Kurdistan Region/Iraq

ABSTRACT. According to Newton's laws of motion the interaction between two planets produces a motion that can be described by Kepler's laws. Kepler's second law (Law of area's), indicates that the force associated with the gravitational interaction is central. At the time of the total Solar Eclipse, the Moon enters totally over the joining line between the Sun and the earth, changing the resultant value of the attraction forces between these three planets (The Sun, Earth, and Moon).In the present work we tried:

(1). A. To study the effect of Solar Eclipse of 1999 August 11 on the value of gravitational acceleration (g) in Sulaimani and Hawler.
B. To prove that the Eclipse in Sulaimani was total.

(2). To study some optical characteristics of the Solar Eclipse of 1999 August 11 from which we specified the direction of the slits at the surface of the Moon with respect to Kurdistan region.

Introduction

Galileo was the first person who has performed in 1590 the experiment of dropping a cannon and a musket ball from the leaning Tower of Pisa, which, contrary to the teaching of Aristotle, reached the ground simultaneously. He thus clearly showed that all bodies irrespective of their mass or nature falling freely in vacuum, have the same acceleration at a given place. This acceleration is called acceleration due to gravity (g) as it is due to the gravitational attraction of the body by the earth towards its center. It is numerically equal to the weight of unit mass [1]. The value of (g) differs from place to place being the greatest at the poles (983.245 cm/sec.^{2}) and the least at the equator (978.16 cm/sec.^{2}) with intermediate values in between [2]. Its value for all practical purpose is however taken to be (980 cm/sec.^{2}) Due to this comparatively large value of (g) bodies fall much too quickly to the surface of the earth when dropped freely, and hence it becomes difficult to measure it directly with any great accuracy. We therefore, determined it indirectly with the help of a simple pendulum. For this purpose Galileo noticed a swinging lamp in the Cathedral at Pisa and timed oscillation against his own pulse beats. The time taken for each swing was found to be the same.

Variation of the value of (g)

The value of (g) at a given place is affected by a number of factors:

1.The latitude
   a. Rotation of the earth
   b. The bulge of the equator
2.The altitude
3.The elevated masses
4.The depth
5.The topographical effects.

The value of (g) at a point is also affected to some slight extent by local causes even by masses like buildings in the neighborhood of the region. It is also affected by time [1].

In this paper we add the effect due to Solar Eclipse to the above factors since the local and temporal change in the value of (g) in this case is not less than the change caused by the above mentioned factors, particularly in case of the Total Solar Eclipse. No importance has been accorded to this in relevant literature Solar.

Experimental

(1) A. We used a simple pendulum for obtaining the gravitational acceleration at 15.51 p.m local time on Wednesday, August 11, 1999 in Sulaimani.

One million citizen witnessed 1.5 minute total Eclipse and felt a gentle breeze accompanying when the Moon cast its dark shadow upon the area.

A copper bob of diameter 4.94 cm suspended on a thin length L has been used as approximation to a simple pendulum, the period of one oscillation (T) from time of 20 oscillations has been obtained at L=50 cm, by using the simple pendulum equation :

$$g=4\pi L/T^2 \qquad (1)$$

The value of (g) obtained was only 978.8 cm/sec.^{2} . By using the same equipment at the same place the average value of (g) calculated for several days later equal to 979.8 cm/sec.^{2}

We calculated the value of (g) also from the value of the atmospheric pressure registered by the Meteorological station of Sulaimani (1) and Hawler (2), the formula used for calculating (g) from their data is as follows: $P=\rho gh$, where P is the atmospheric pressure, ρ is the density of mercury 13.6 kg/m^3, h is the mercury column height.

The calculated values of (g) at the time of total Solar Eclipse were 979.76 cm/sec.^{2} in Sulaimani, and 979.78 cm/sec.^{2} in Hawler, as it is shown in (Table 1), (Fig 1) and (Table2), (Fig2) respectively.

(1) Sulaimani : Latitude 035^0 35 N
Longitude 045^0 27 E
Altitude 834.8 m

(2) Hawler : Latitude 36^0 7 30 N
Longitude 044^0 1 15 E
Altitude 415 m

Table 1

The time	P(mbar)	H(mmHg)	g(cm.sec^2)
14:40	955.9	717.1609075	980.0696600
15:00	955.6	716.9358335	980.0696600
15:15	955.4	716.785784	980.0785358
15:30	955.3	716.9358335	979.7619700
15:45	955.3	716.9358335	979.7619700
16:00	955:3	716.9358335	979.7619700
17:00	955.3	716.9358335	979.7619700
18:00	955.6	716.9358342	980.0696500

Fig(1)

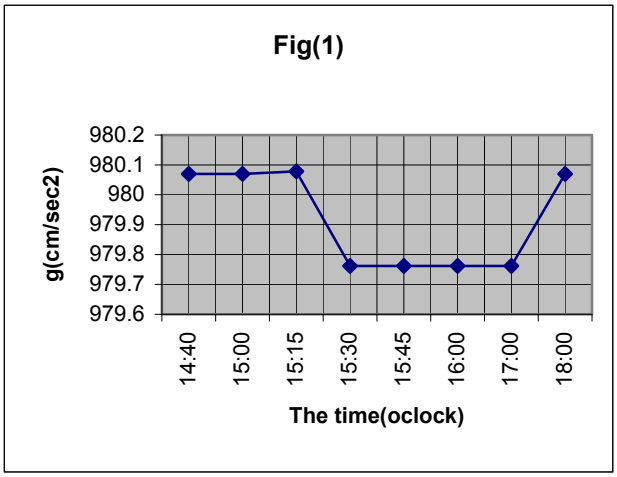

Table 2

The time p.m	P(mbar)	H(mmHg)	g(cm.sec.)^2
12:00	909.1	682.0493386	980.06968
13:00	909.1	682.0493386	980.06968
16:00	907.7	680.9989931	979.78
17:00	907.7	680.9989931	979.78
19:00	907.6	680.9239685	980.06968
20:00	907.6	680.9239685	980.06968

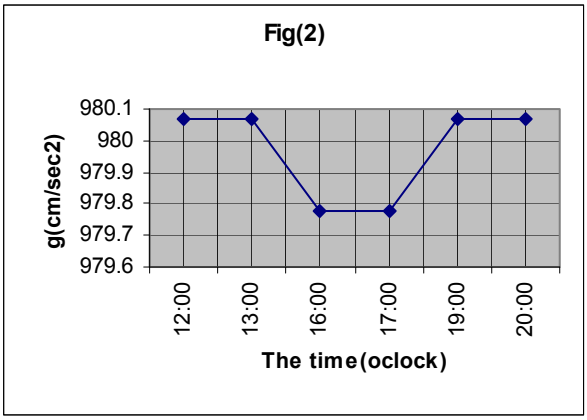

(1).B. To prove that the Eclipse was total in Sulaimani area an experiment with a boiled egg was carried out through the duration of the Solar Eclipse of 1999 August 11.

Throughout the whole period of the total Eclipse (1.5 min.) the boiled egg stood completely erect, as shown on Fig.(3), as soon as the process of the Sun re-emerging started the egg equilibrium was over as shown on Fig.(4).

Fig(3) The stood of the boiled egg completely erect at 15.50,p.m local time in Sulimani.

This study depended on the meteorological data (atmospheric pressure) received from the Meteorological stations in Sulaimani an Hawler (Arbil). On the basis of the above data the gravitational acceleration in the area was calculated.

Fig(4) Starting of the sun re-emerging.

During the experiment it was observed that the gravitational acceleration had been reducing from the start of the Solar Eclipse reaching the lowest point 979.761 cm/sec.^{2} in Sulaimani between 15:30 and 17:00 p.m, local time as shown in table (1). In Sulaimani the Total Solar Eclipse started at 15:50 p.m, local time and lasted more than 1.5 min., at the time of total Solar Eclipse in Sulaimani, from the simple pendulum experiment, the calculated value of (g) is only 978.8 cm/sec.^{2}

In Arbil the lowest value of gravitational acceleration was 979.780 cm/sec.^{2} between 16:00 and 17:00 p.m, local time as shown in table (2). In Arbil the total Solar Eclipse started at 15.49 p.m, local time and continued for 1.5 min.

Gravitational acceleration is one of the parameters, which shows the totality of an Eclipse. When the gravitational acceleration value reached its lowest value (979.780 cm/sec.^{2}) the boiled egg stood erect.

Although according to NASA prognosis (4) the total Eclipse in the area was in Mosul North of Sulaimani however the reduction in value of (g) and the stood of the boiled egg erect proves that the Solar Eclipse in Sulaimani was also total.

2-Some Optical Characteristics of Solar Eclipse of 1999 August 11

Immediately before the total disappereance of the Sun and also immediately after its revealing the following phenomenon, which lasted for a few seconds, was observed around us in Sulaimani, a colored shadow that was running quickly on every object.

The above phenomenon is due to the fact that the edge of the Moon is not perfectly round, there for light passes through the slits in the edge of the Moon is diffracted,and undergoes dispersion resulting that colored shadow.

The colored fringes has been compared with the fringes obtained from Fraunhofer diffraction by a single opening, the result showed that the edge of the Moon contains rectangular apertures which are very long compared to their widths, and their directions must be perpendicular to the direction of the moving shadow.

Fig. 5 represents a section of a slit of width e illuminated by parallel light of wavelength λ, incident from the left perpendicular to the plane π_1 of the slit. Huygens secondary spherical wavelets [6] can be through of as being sent out from every point on the wave front at the instant that it occupies the plane of the slit.

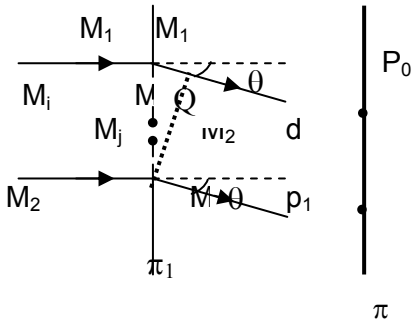

Fig. 5 Geometrical construction for investigation the intensity in the single-slit diffraction pattern

The maximum intensity of the strong central band comes at the point p_o on the screen π where evidently all secondary waves normally to the plane of the slit as MM_1, M_2M_2 will be focused.

Those that travel at any angle θ as M_1M_1,M_2M_2 will reach p_1, which is in the focal plane of a convergent lens.

The amplitude of resulted vibrations at p_1 depend on the path difference between them, e.g for M1M1 and M2M2 is M1Q= esinθ= 2k λ/2, where e= M1M2.

To obtain zero intensity at a point the following relation must be satisfied:

$$M_1 Q = e \sin\theta = 2k\lambda/2 \quad \text{or} \quad \sin\theta = k\lambda/e \tag{2}$$

From the principle maximum, the intensity falls to zero, then passes through several secondary maxima with approximately equally spaced points of zero intensity [7].

Analytically the distribution of the intensity from Fraunhofer diffraction by a slit, can be obtained [8,9] by the relation (3)

$$E_\theta = E_0 \frac{\sin^2 u}{u^2} \tag{3}$$

where

$$u=(\pi e \sin\theta)/\lambda$$

At p_0 where u=0

$$E_\theta = \lim_{u\to 0} E_0 \frac{\sin^2 u}{u^2}$$

and $E_\theta=E_0$ is the amplitude when all the wavelet arrive on π plane in phase.The diffraction pattern given by (3) is illustrated in fig. 6

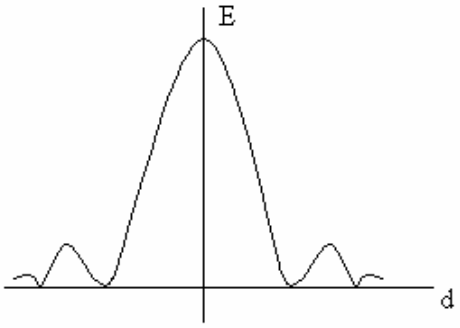

Fig. 6.Amplitude contours for Fraunhofer diffraction of a single slit

The above result is correct when the slit is very long, compared to its width: L>>e

Where L is the length of the slit.

For a slit of comparable width e and length L, the expression for the intensity is:

$$I = e^2 L^2 \frac{\sin^2 u}{u^2}\frac{\sin^2 \gamma}{\gamma^2} \qquad (4)$$

Where

$\gamma=\pi L\sin\Omega/\lambda$ and $u=\pi e\sin\theta/\lambda$

The angles θ and Ω are measured from the normal to the aperture at its center in planes through the normal parallel to the side e and L respectively.

The diffraction pattern given by Eq(4) when e and L are comparable with each other is illustrated in fig. 7. The intensity in the pattern is concentrated principally in two directions coinciding with the sides of the aperture and in each of these directions it corresponds to the simple pattern for a slit width equal the width of the aperture in that direction, the fringes are more closely spaced in the direction of the longer dimension of the aperture .

For a slit having L very large the factor $\sin^2\gamma/\gamma^2$ in eq.(4) is zero for all values of Ω except extremely small ones, this means that the diffraction pattern is limited to a line on the screen perpendicular to the slit and resembles a section of the central horizontal line of bright spots in fig.7 .

For white light, the diffraction phenomenon is acompanies with the phenomenon of dispersion. The angle of diffraction for the rays that produce the bright fringes depends on λ, it is larger for the longer wavelength, consequently, the central maximum is a white fringe, while the secondary maxima are colored, a violet fringe near the central maximum and a red fringe in the exterior alternatively was moving.

At the time of Eclipse the sun acts as a white light source that illuminates the Moon's edges that act as rectangular apertures of length L and width e where L>>e, therefore, the intensity of the colored fringes on

earth objects acting as a screen was represented by the central horizontal colored spotted line on fig. 7. Each point of the slit source (the Moon edges) forms a line pattern that falls adjacent to each other on every object running quickly with the velocity of the Moon's umbra, indicating that L>>e, consequently from the direction of the colored shadow that was moving from North to South of Sulaimani we conclude that the direction of the slits on the edge of the Moon was directed from North towards the South of Kurdistan.

From the diffraction pattern observed at the time of Eclipse we conclude that the diffraction of the slits on the edge of the Moon was directed from North towards the South of Kurdistan.

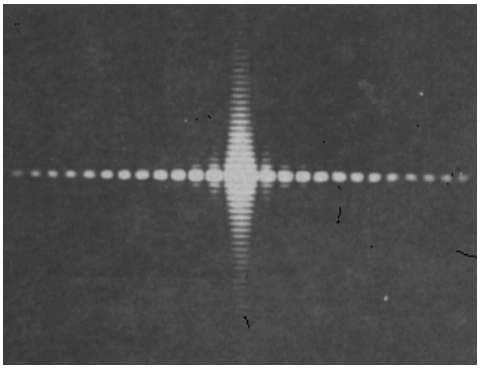

Fig.7 Diffraction pattern from a rectangular opening.

Conclusion

This study depended on the meteorological data (atmospheric pressure) received from the Meteorological stations in Sulaimani an Arbil. On the basis of the above data the gravitational acceleration in the area was calculated.

During the experiment it was observed that the gravitational acceleration had been reducing from the start of the Solar Eclipse reaching the lowest point 979.761 cm/sec^2 in Sulaimani between 15.30 and 17.00 p.m, local time as shown in table (1). In Sulaimani the total Solar Eclipse started at 15.50 p.m, local time and lasted more than 1.5 min, at the time of total Solar Eclipse. From the simple pendulum experiment, the calculated value of (g) is only 978.8cm /sec^2.

In Arbil the lowest value of gravitational acceleration was 979.780 cm/sec^2 between 16.00 and 17.00 p.m, local time as shown in table (2). In Arbil the total Solar Eclipse Started at 15.49 p.m, local time and continued for 1.5 min.

Gravitational acceleration is one of the parameters, which shows the totality of an Eclipse. When the gravitational acceleration value reached its lowest value (979.780 cm/sec.^{2}) the boiled egg stood erect.

Although according to NASA prognosis (4) the total Eclipse in the area was in Mosul North of Sulaimani however the reduction in value of (g) and the stood of the boiled egg erect proves that the Solar Eclipse in Sulaimani was also total.

From the difraction pattern observed at the time of eclipse we conclude that the direction of the slits on the edge of the Moon was directed from North towards the South of Kurdistan.

REFERENCES

1- D.S Mathur, *Element of properties of matter*, Shyam Lalcharitable Trust Ram Nigar,New Delhi-55 (1969)

2- K.K. Ruderman,H. Moyer,*Berkeley physics course vol.1 Mechanics*, Mc Graw-Hill publishing company (1973)

3- A. James, J. R. Richards, F. W. Sears and M. W. Zemansky, *Modern Uneversity Physics*, Addison.Wesley (1960)

4- Eclipse Predictio&WebMaster: Fred Espenak,
e-mail: mailto:espenak lepvax.gsfc.nasa.gov
Official NASA Representative: Dr. Drake Deming
e-mail: drake tecate.gsfc.nasa.gov
Planetary Systems Branch–Code 693
NASA/Goddard Space Flight Center, Greenbelt, Maryland 20771 USA

5- F.Espenak and J.Anderson, Solar Eclipse of 1999 August 11,NASA PR 1398 (1999)

6- F. W. Sears, *Optics*, Addison-Wesliy Publishing Company, (1958)

7- A. F. Jenkins and H.E.White,*Fundamentals of Optic*, Mc Graw-Hill (1973)

8- R. Titeica and I. Popescu, *Fizica*, Editura Tehnica, Bucuresti (1973)

9- R.W.Wood, *Physical Optics* ,The Macmillan Company, New York (1921),